NASA/TM—2015–218877

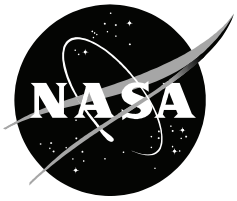

Shake Test Results and Dynamic Characterization of the Large Rotor Test Apparatus in the NFAC 40- by 80-Foot Wind Tunnel

Carl R. Russell
Ames Research Center
Moffett Field, California

September 2015

NASA STI Program ... in Profile

Since its founding, NASA has been dedicated to the advancement of aeronautics and space science. The NASA scientific and technical information (STI) program plays a key part in helping NASA maintain this important role.

The NASA STI program operates under the auspices of the Agency Chief Information Officer. It collects, organizes, provides for archiving, and disseminates NASA's STI. The NASA STI program provides access to the NTRS Registered and its public interface, the NASA Technical Reports Server, thus providing one of the largest collections of aeronautical and space science STI in the world. Results are published in both non-NASA channels and by NASA in the NASA STI Report Series, which includes the following report types:

- TECHNICAL PUBLICATION. Reports of completed research or a major significant phase of research that present the results of NASA Programs and include extensive data or theoretical analysis. Includes compilations of significant scientific and technical data and information deemed to be of continuing reference value. NASA counterpart of peer-reviewed formal professional papers but has less stringent limitations on manuscript length and extent of graphic presentations.

- TECHNICAL MEMORANDUM. Scientific and technical findings that are preliminary or of specialized interest, e.g., quick release reports, working papers, and bibliographies that contain minimal annotation. Does not contain extensive analysis.

- CONTRACTOR REPORT. Scientific and technical findings by NASA-sponsored contractors and grantees.

- CONFERENCE PUBLICATION. Collected papers from scientific and technical conferences, symposia, seminars, or other meetings sponsored or co-sponsored by NASA.

- SPECIAL PUBLICATION. Scientific, technical, or historical information from NASA programs, projects, and missions, often concerned with subjects having substantial public interest.

- TECHNICAL TRANSLATION. English-language translations of foreign scientific and technical material pertinent to NASA's mission.

Specialized services also include organizing and publishing research results, distributing specialized research announcements and feeds, providing information desk and personal search support, and enabling data exchange services.

For more information about the NASA STI program, see the following:

- Access the NASA STI program home page at http://www.sti.nasa.gov

- E-mail your question to help@sti.nasa.gov

- Phone the NASA STI Information Desk at 757-864-9658

- Write to:
  NASA STI Program
  STI Support Services
  Mail Stop 148
  NASA Langley Research Center
  Hampton, VA 23681-2199

NASA/TM—2015–218877

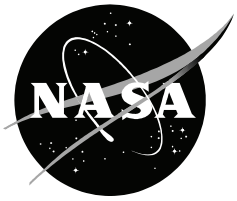

Shake Test Results and Dynamic Characterization of the Large Rotor Test Apparatus in the NFAC 40- by 80-Foot Wind Tunnel

Carl R. Russell
Ames Research Center
Moffett Field, California

National Aeronautics and
Space Administration

Ames Research Center
Moffett Field, CA 94035-1000

September 2015

Available from:

NASA Center for AeroSpace Information
7115 Standard Drive
Hanover, MD 21076-1320
443-757-5802

National Technical Information Service
5301 Shawnee Road
Alexandria, VA 22312
703-605-6000

This report is also available in electronic form at

http:/ntrs.nasa.gov

TABLE OF CONTENTS

LIST OF FIGURES

LIST OF FIGURES (cont.)

LIST OF TABLES

NOMENCLATURE

FEA	Finite Element Analysis
FRF	Frequency Response Function
LRTA	Large Rotor Test Apparatus
LVDT	Linear Variable Differential Transformer
NASTRAN	NASA Structural Analysis Program
NFAC	National Full-Scale Aerodynamics Complex
RTA	Rotor Test Apparatus
SBMR	Sikorsky Bearingless Main Rotor
AFxxx	FRF from input force to axial force balance gauge at xxx azimuth
α	Shaft angle of attack, positive aft, deg
F_{out}/F_{in}	Calculated FRF from input force to output force
g_{out}	Measured output acceleration, g
M_{out}/M_{in}	Calculated FRF from input moment to output moment
N	Rotor harmonic number
NFxxx	FRF from input force to normal force balance gauge at xxx azimuth
SFxxx	FRF from input force to side force balance gauge at xxx azimuth

SHAKE TEST RESULTS AND DYNAMIC CHARACTERIZATION OF THE LARGE ROTOR TEST APPARATUS IN THE NFAC 40- BY 80-FOOT WIND TUNNEL

Carl Russell[1]

Ames Research Center

ABSTRACT

Prior to the full-scale wind tunnel test of the UH-60A Airloads rotor, a shake test was completed on the Large Rotor Test Apparatus. The goal of the shake test was to characterize the oscillatory response of the test rig and provide a dynamic calibration of the balance to permit accurate measurement of vibratory hub loads. This paper provides a summary of the shake test results, including balance, shaft bending gauge, and accelerometer measurements. Sensitivity to hub mass and angle of attack were investigated during the shake test. Hub mass was found to have an important impact on the vibratory forces and moments measured at the balance, especially near the UH-60A 4/rev frequency. Comparisons were made between the accelerometer data and an existing finite-element model, showing agreement on mode shapes, but not on natural frequencies. The results suggest that the shake test data can be used to correct in-plane loads measurements up to 10 Hz and normal loads up to 30 Hz.

INTRODUCTION

A shake test of the Large Rotor Test Apparatus (LRTA) was performed at the National Full-Scale Aerodynamics Complex (NFAC) in an effort to enhance NASA's capability to measure dynamic hub loads for full-scale rotor tests. This paper documents the complete results of the shake test, including frequency response data for the LRTA balance and output shaft bending gauges, as well as for accelerometers mounted on the LRTA and its support struts.

Oscillatory hub loads are the primary source of vibration in helicopters and other rotorcraft, leading to passenger discomfort and structural damage due to fatigue of aircraft components. The problem of both measuring and mitigating dynamic loads on rotorcraft airframes is not a new one; reference 1 provides a good overview of the history of the helicopter vibration problem. There are currently novel methods being developed to reduce rotor vibrations, and the experimental capability to measure dynamic loads on a full-scale rotor in a wind tunnel is key to understanding how well these methods work. NASA conducts full-scale wind tunnel tests on rotors using the LRTA and other test stands in the NFAC, so the capability to measure dynamic loads on these test stands is important.

In order to measure rotor forces on the LRTA, a balance system in the nonrotating frame is used. The forces at the balance can then be translated to the hub reference frame to obtain measured rotor loads. Reference 2 provides a detailed description of the LRTA and its balance. Because the LRTA has its own dynamic response, measuring dynamic loads requires that the balance be calibrated to compensate for the natural frequencies of the test rig. A shake test is necessary to complete this calibration.

---

[1] Aerospace Engineer, Rotorcraft Aeromechanics, Carl.R.Russell@nasa.gov

As part of the UH-60A Airloads wind tunnel test (ref. 3), a large shaker system was used to excite the LRTA at frequencies up to 100 Hz. In addition to measurements from the balance and shaft bending gauges, the LRTA and its support struts were instrumented with accelerometers to measure the dynamic response of the entire test rig. The purpose of collecting accelerometer measurements was to provide data that could be validated against a finite element model of the LRTA. Results of the shake test, as well as comparisons with a finite element analysis, are presented in this paper. The ultimate goal is to use the data, along with mathematical models of the LRTA, to generate a dynamic calibration of the balance. An accurate dynamic calibration could then be used to correct measured oscillatory hub load data acquired during testing. A simple calibration has been performed using the data from this shake test, and the results are presented in reference 4.

BACKGROUND

A similar shake test and dynamic calibration effort was performed on the Rotor Test Apparatus (RTA), a smaller test stand also used in the NFAC for full-scale rotor testing (refs. 5–6). The RTA dynamic calibration effort investigated the effects of several variables on frequency response, including hub mass, pre-load, pre-load angle, and rotation of the rotor shaft. A key finding of the RTA shake test was that hub mass had the largest effect on the dynamic response. For that test, two hub masses were tested, representing the weight of a BO105 four-bladed hingeless rotor and a Sikorsky five-bladed Bearingless Main Rotor (SBMR). The weight difference between these two rotors was 740 lb, and this change was enough to move the highest peak in the frequency response function (FRF) for side force from approximately 16 Hz for the BO105 rotor mass down to 13 Hz for the heavier SBMR mass. The magnitude of this peak was approximately double for the heavier rotor. These results made it clear that if a dynamic calibration of the RTA balance was going to be based on shake test results alone, the mass of the rotor would need to be accurately represented. With this knowledge, the dynamic calibration obtained for the RTA was subsequently used with some success to estimate dynamic hub loads on the SBMR (ref. 7).

Prior to the current shake test, the dynamic response of the LRTA and its balance had never been extensively measured. There were two shake tests performed on the LRTA installed in the NFAC: one in the 80- by 120-foot test section, and one in the 40- by 80-foot test section. The primary objective of both of these tests was to determine the potential of ground resonance instability, and measuring the balance response was left as a secondary objective. Therefore, neither of these tests provided sufficient data to attempt a dynamic calibration of the balance. The results of the shake test in the 80- by 120-foot test section are detailed in reference 2.

One approach that has been proposed for obtaining a valid dynamic calibration of the balance is to use a detailed finite element analysis (FEA) model of the LRTA. If the FEA model can be tuned to match the experimental shake test data, then it should be possible to generate transfer functions from the hub input forces to the balance measurements. This correlation process has in the past been very time intensive, but there has been recent success in tuning FEA models to match shake test data using optimization techniques (ref. 8).

TEST DESCRIPTION

The shake test was carried out in the 40- by 80-foot test section of the NFAC prior to the UH-60A Airloads test. The LRTA was mounted on the NFAC's 8-foot struts with 33-inch strut tips—the same as those used during the actual wind tunnel test. The UH-60A shaft extender and hub were mounted on the LRTA output shaft, and the "instrumentation hat" was mounted on top of the hub, but the rotor blades were not present. An adapter was placed on top of the hub to facilitate vertical shaking. A hydraulic shaker system provided both in-plane and vertical excitation, and frequency response data were collected for the balance, rotor shaft bending gauges, and multiple accelerometers on the LRTA. The following sections describe in detail the various systems and pieces of hardware that were used to perform the shake test.

Measurement Hardware and Instrumentation

The LRTA balance is made from a stainless steel ring that is 18 inches high by 49 inches in diameter. This ring has four machined cutouts leaving four symmetrically placed rectangular flexure posts separating an upper (metric side) and lower (non-metric side) ring. The lower ring sits on the LRTA transmission, and the upper ring supports the output shaft housing, which in turn supports the output shaft through two sets of bearings. Each of the flexure posts is instrumented with strain gauges measuring normal, axial, and side force. The forces measured at the flexures are typically combined to measure the overall rotor normal, axial, and side forces, along with pitch and roll moments at the hub; the balance does not measure rotor shaft torque moments. There are two sets of gauges on the balance, a primary and a backup set, for a total of 12 primary and 12 backup gauges. A schematic of the balance with the sign conventions for balance forces and moments is shown in Figure 1.

For this shake test, the 12 primary balance gauges were used to collect loads data, with a separate data channel dedicated to each balance gauge. For the RTA dynamic calibration reported in references 5 and 6, data were not collected for the individual balance gauges; instead, the gauge forces were resolved into balance forces and moments, which were then collected and analyzed. Unlike the RTA test, the approach with the current shake test of the LRTA was to collect the individual gauge measurements so that dynamic gauge interaction terms could be determined.

When mounted on the LRTA, the UH-60A hub is supported by a two-part output shaft. The lower output shaft section is integral to the LRTA, and the upper part is a shaft extender identical to the one found on the UH-60A. The two shafts mate together via a spline interface. There are two bending strain gauges mounted on the LRTA output shaft and two on the UH-60A shaft extender that can be used together to measure in-plane loads and pitching and rolling moments at the hub. These bending gauges provided additional loads measurements during the shake test, which were later compared to the results for the balance gauges.

To help with validation of existing NASTRAN (ref. 9) models of the LRTA, 47 accelerometers were placed at various locations on the test rig. All of the accelerometers were Kistler model 8628B5, rated at ±5g with 2 kHz bandwidth. The accelerometers were located on the LRTA chassis, as well as at the bases and tips of the support struts. Additional accelerometers were placed in the instrumentation hat and on the vertical shake plate. For in-plane shaking, an accelerometer was placed at the point of load application on the bifilar arm, parallel to the loading direction. The placement and directions of the accelerometers are shown in Figure 2. The approximate locations of the accelerometers are contained in Table A1 in Appendix A. Some of the accelerometers were relocated during testing, and Table A2 lists their run-by-run locations.

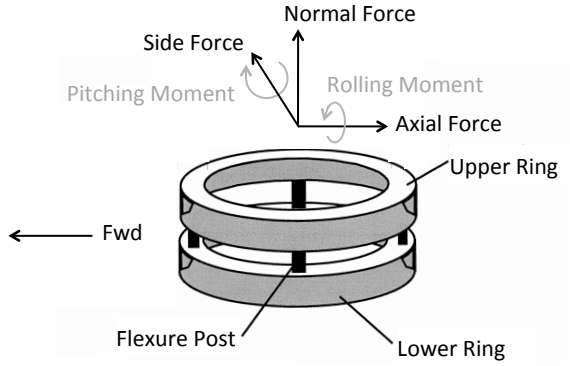

Figure 1. Schematic of LRTA rotor balance.

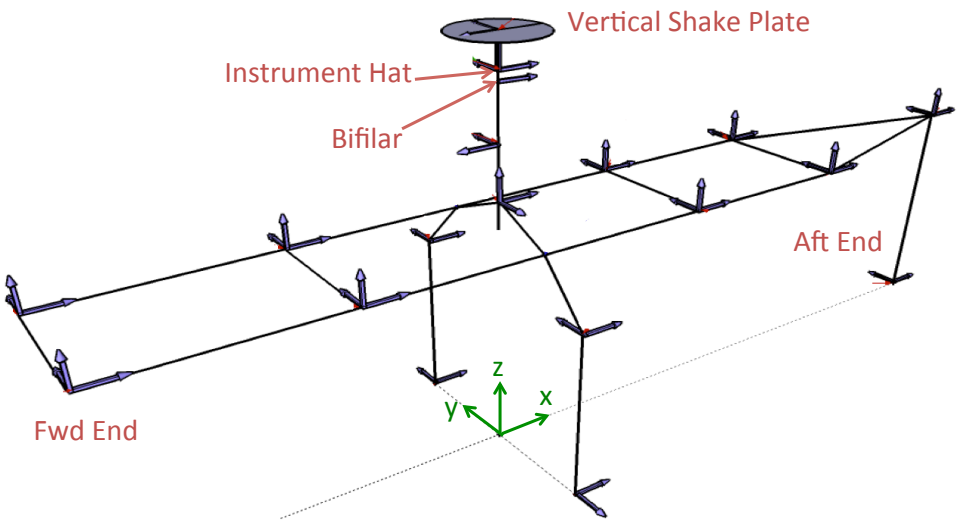

Figure 2. Shake test accelerometer locations.

Hydraulic Actuator System and Shake Hardware

A hydraulic actuator system provided the shaking force for this test. The point of application of in-plane oscillatory loads was the hub bifilar arm that leads blade 1. None of the bifilar weights were present for this test. A metal fixture was clamped onto the bifilar arm to provide an attachment point for the hydraulic shaker.

In order to facilitate shaking in the vertical direction, an adapter, referred to as the "vertical shake plate" throughout this document, was fitted to the hub. The vertical shake plate weighed 384 lb and was installed for all but two of the test runs. Two hundred pounds of lead weights could also be attached to the vertical shake plate to help evaluate the sensitivity of the dynamic response to hub mass. The UH-60A hub and shaft extender together weighed approximately 800 lb, so the addition of the vertical shake plate and the lead weights represent a significant increase in weight at the hub. This increase is comparable in magnitude to the total weight of the UH-60A blades.

The hydraulic actuator was backstopped against an 11,780-lb reaction mass, which was hung from the bridge crane in the 40- by 80-foot test section and secured by guy-wires to the wind tunnel floor. For in-plane shaking, a 6-foot extension beam was attached to the reaction mass to provide spacing from the LRTA and allow for tie-down attachment. For vertical shaking, the extension beam was not necessary, and the reaction mass was attached directly to the actuator. An Interface 1010AF-1K load cell, capable of measuring loads of ±1,000 lb was attached in series with the actuator and the reaction mass to measure the input loads.

The shaking force was applied by an MTS Model 204.08 hydraulic actuator connected to a Moog G761 servo-valve. An MTS Model 407 Controller with an external function generator provided the input to the servo-valve. The shaker was operated in stroke-feedback mode, with a linear variable differential transformer (LVDT) providing the controller with position data for the shaker piston. The input loads consisted of a random signal with the waveform provided by the data acquisition system. The input signal was routed to the shaker controller through a manually adjustable amplifier. The amplifier gain was adjusted to achieve a shaker signal that provided enough energy to the system without exceeding any safety limits. The amplitude of the input loads varied from run to run, but the maximum for any run was ±800 lb.

To protect the hub from damage during the shake test, the hub arms and bifilar were instrumented with strain gauges. These strain gauge channels were monitored throughout the test, and they would automatically trigger an emergency stop that would dump hydraulic pressure from the shaker system if safety limits were exceeded. A maximum allowable input force of ±1,000 lb was set for the load cell as well. The emergency stop could also be triggered manually if there was a visible safety issue. The shaker setup is shown in Figures 3–5.

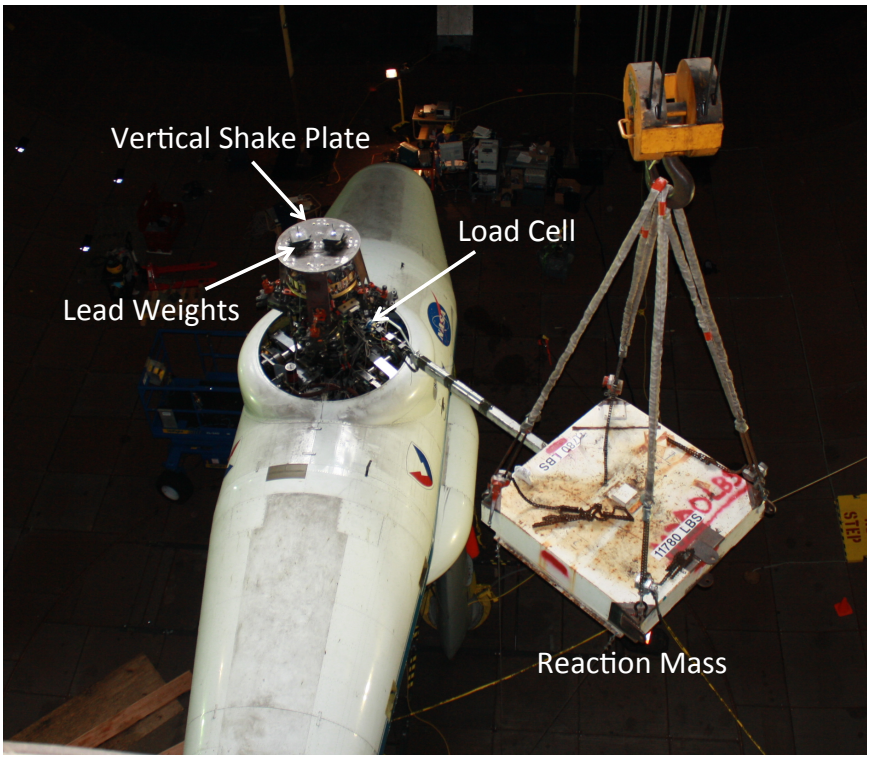

Figure 3. Shake test installation. In-plane shaking at 50-deg azimuth.

Figure 4. Shake test installation. Vertical shaking on the hub centerline.

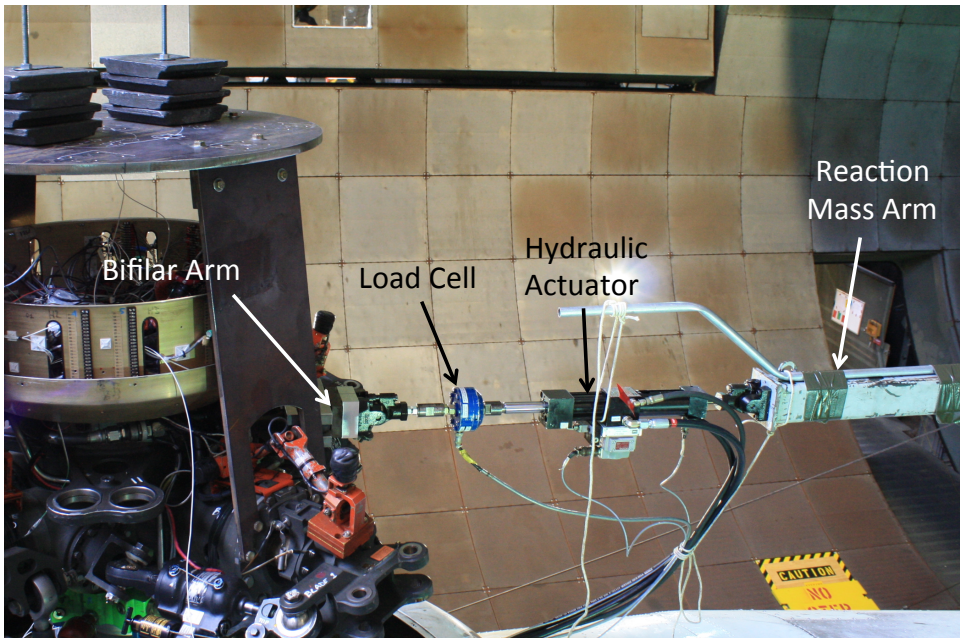

Figure 5. Close-up of load cell and actuator installation.

Data Acquisition System

The data acquisition system for the shake test consisted of an HP E8400A VXI mainframe containing four HP E1432A cards and an NI MXI-2 controller card. Each of the E1432A cards can acquire 16 channels of data at up to a 51.2-kHz sampling rate, allowing 64 channels to be sampled simultaneously for this test. Twelve channels were used for the balance gauges, 4 for the shaft bending gauges, and 1 for the shaker load cell, leaving 47 channels available for accelerometers. The E1432A includes a digital signal processor, allowing onboard calculation of frequency response functions. The E1432A cards are also capable of outputting an arbitrary waveform without sacrificing an input channel, and this feature was used to generate the signal for the hydraulic shaker. The data acquisition system was controlled via the MXI-2 card by MTS IDEAS v9 software running on a Windows 2000 desktop computer.

All of the FRFs were generated using a random signal as input, and the input signal settings are tabulated in Appendix A in Table A3; note that in some cases not all of the settings were documented. The data-sampling rate for this test was 32.8 kHz. Digital low-pass filtering and down-sampling were applied, giving a final sample rate of 204.8 Hz. Frequency response functions and coherence were recorded for all channels over a frequency range of 0 to 80 Hz, with a spectral resolution of 0.1 Hz. The FRFs were constructed by averaging 50, 10-second frames of data per run. The FRFs for the balance and shaft bending gauges were recorded in volts out per pound in, and then converted to engineering units during post-processing. The accelerometer FRFs were recorded in *g*'s out per pound in.

The balance and shaft bending gauge signals, as well as the safety monitoring channels, were routed to the NFAC control room for signal conditioning. All channels routed through the control room were filtered with a 4-pole Butterworth low-pass filter with a 1,000-Hz cutoff frequency. From the control room, these channels were routed back to the test section. The balance and shaft-bending gauge channels went to the data acquisition system, and the hub arm and bifilar strain gauge channels were connected to both an Astro-Med data acquisition system for real-time monitoring and the hydraulic control system for emergency-stop triggering. The accelerometer signals were routed to the data acquisition system through 4 Kistler 5124A1 Piezotron couplers, each with a capacity of 12 channels. The accelerometer channels did not receive low-pass filtering prior to data acquisition. The accelerometer bandwidth is only 2 kHz (well below the sampling frequency of 32.8 kHz), but with no low-pass filtering applied, there is potential for aliasing from electrical noise above approximately 16 kHz. The signal-to-noise ratio of the accelerometers used for this test is very good, so the risk of aliasing from such high frequencies was deemed acceptably low.

Test Conditions

The conditions tested are summarized in Table 1. Table A3 in Appendix A gives a complete listing of the test runs. Note that only five forces and moments were investigated for this study; none of the loading scenarios included yaw moments. In-plane loads were applied at four azimuths to determine the response of the LRTA to different combinations of side and axial forces. The in-plane loads were applied at the bifilar, which is 7.3 inches above the hub plane. The same bifilar arm was used for all in-plane shaking, so the hub was rotated and locked out for each in-plane shake azimuth. Vertical loads were applied along the hub axis to obtain the pure normal load response. Off-center vertical loads were applied at three azimuthal locations and a radius of 15 inches from the hub axis to determine the response to pitch and roll moments. The top of the vertical shake plate, where the vertical loads were applied, was 31.7 inches above the hub plane. The hub was not rotated between vertical shake runs; instead, the vertical shake plate had multiple attachment points so that the load could be applied at multiple locations. The hub azimuth for each run is documented in Table A3 of Appendix A.

Table 1. Shake test matrix. Shaking direction is indicated as in-plane or vertical along with the azimuth of shake application.

Configuration	In-Plane Shake Azimuth (deg)	Vertical Shake Location (deg)
Without shake plate	0, 270	—
With shake plate	0, 270, 315, 50	Center, 0, 270, 315
With shake plate plus 200-lb mass	0, 270, 315, 50	Center, 0, 270, 315
With shake plate and LRTA 10 deg nose down	270	—

The majority of testing was performed with the vertical shake plate attached to the hub and with the LRTA at 0-deg pitch. Two additional runs were performed at the end of the test with the shake plate removed to determine its effect on the frequency response. The effect of angle of attack was also considered, and a run was performed with the LRTA at an alpha of –10 deg (LRTA nose down).

SHAKE TEST RESULTS

Numeric results for all shake test runs are contained in Appendix C, a separate volume. The data in the appendix include frequency response functions for all balance gauges, shaft bending gauges, and accelerometers. Coherence data for each sensor are also tabulated. Appendix C also contains data for a brief rap test that was conducted after the shake test was completed. The main body of this report gives sample plots of the FRF data as well as plots of forces and moments resolved from the balance and bending gauge measurements. Results are first presented for the balance gauges and shaft bending gauges. The accelerometer data are presented in the following section.

Balance Results

Results are presented here for a subset of the loading scenarios given in Table 1. Results for the individual gauge forces are given first. The gauge forces are then resolved into forces and moments in the balance axes using the following equations:

$$
\begin{aligned}
Axial\ Force\colon\ \frac{F_{out}}{F_{in}} &= \frac{\mathrm{AF000} + \mathrm{AF090} + \mathrm{AF180} + \mathrm{AF270}}{\cos(\psi)} \\
Side\ Force\colon\ \frac{F_{out}}{F_{in}} &= \frac{\mathrm{SF000} + \mathrm{SF090} + \mathrm{SF180} + \mathrm{SF270}}{\sin(\psi)} \\
Normal\ Force\colon\ \frac{F_{out}}{F_{in}} &= \mathrm{NF000} + \mathrm{NF090} + \mathrm{NF180} + \mathrm{NF270} \\
Roll\ Moment\colon\ \frac{M_{out}}{M_{in}} &= \frac{(\mathrm{NF270} - \mathrm{NF090}) * 1.827}{L_F \sin(\psi)} \\
Pitch\ Moment\colon\ \frac{M_{out}}{M_{in}} &= \frac{(\mathrm{NF180} - \mathrm{NF000}) * 1.827}{L_F \cos(\psi)}
\end{aligned}
\tag{1}
$$

where AFxxx, SFxxx, and NFxxx are the transfer functions from input force (measured at the load cell) to the given balance gauge. The 1.827 in the numerator for the moment equations is the radius, in feet, between the balance flexures. L_F is the moment arm from the shake application point to the balance center. For vertical shaking, L_F is –1.25 feet, and for in-plane shaking, L_F is 5.73 feet. ψ is the azimuth of load application. Note that no gauge interaction terms were included in the calculations for the balance forces and moments. The resolved forces in the balance axes are presented first for in-plane shaking at 0 and 270 deg, and vertical shaking along the hub axis, showing the impact of different masses at the hub. Next, the effects of angle of attack are shown, followed by the impact of shake direction. Finally, pitch and roll moments measured at the balance are discussed.

Individual Gauges and Data Quality

In general, the data quality for the balance gauges is very good, especially for the gauges aligned with the loading direction. Figure 6 shows FRF magnitudes and coherence functions for individual balance gauges for 0-deg in-plane shaking. The balance gauge locations are indicated in Figure 6 by their azimuth and direction (e.g., AF180 is the axial force gauge at 180-deg azimuth). For the axial force gauges shown in Figure 6a, the value of the coherence function for all four gauges is nearly 1.0 over most of the frequency range. There is an antiresonance at 30 Hz, and the coherence at this point drops to nearly zero. For normal force, shown in Figure 6b, the gauges at 0- and 180-deg azimuth show a large response, because axial shaking at the hub imposes a large pitching moment at the balance. The response from the gauges at 90- and 270-deg azimuth is very small, and would ideally be zero if the shake angle was perfect and there was no cross-coupling of the response in the axial and side directions. The coherence for these gauges is therefore relatively poor compared to the axial and NF000 and NF180 gauges. The data quality indicated by the plots in Figure 6 is typical of the balance gauges for all of the runs in this test.

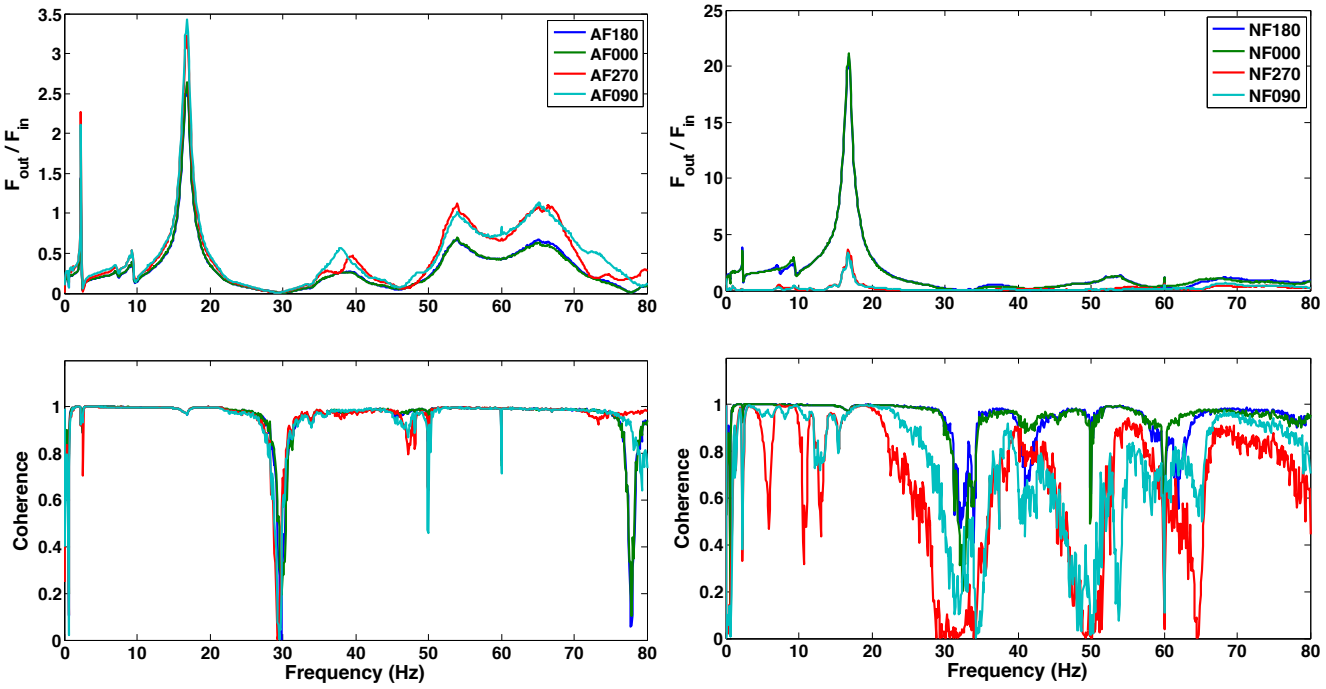

(a) Axial Force Gauges **(b) Normal Force Gauges**

Figure 6. Balance gauge results for 0-deg in-plane shaking; no additional mass on shake plate.

Resolved Forces and Hub Mass Impacts

Figures 7–9 show the effect of hub mass on the magnitude of the frequency response of the resolved forces measured at the balance. As previously stated, for each of the three primary force measurement directions (axial, side, and normal) the forces measured by the four balance gauges were simply summed to obtain the total force. Note that the three plots use the same scale on the y-axis. This is to emphasize the difference in behavior of the LRTA with respect to in-plane versus vertical shaking. The N-per-rev scale on the top of Figures 7–9 is based on the nominal operating speed (258 RPM) of the UH-60A main rotor. Frequency response functions were calculated for frequencies up to 80 Hz. In general, it appears that the shaker did not generate enough energy to excite the LRTA above 40 Hz, so the plots are truncated at 8/rev, or 34.4 Hz. As Figures 7 and 8 clearly show, hub mass has a large effect on the measurement of in-plane loads. There are two strong modes in the axial direction at 13.0 and 17.4 Hz when both the vertical shake plate and the additional 200 lb of mass are present. With the 200 lb removed, a single mode appears at 16.8 Hz, and when the 384-lb vertical shake plate is removed, this mode moves to 25.8 Hz. The results in Figure 8 for shaking in the y-direction show similar behavior, but the natural frequencies are different. Note that the frequencies of these mass-dependent modes in both the x- and y-directions are near 4/rev of the UH-60A rotor.

The accelerometer data, presented later in this paper, were used to identify the mode shapes at various resonant frequencies. The accelerometer data show that bending of the LRTA output shaft is the cause of the mass-dependent mode near 4/rev. The variation in hub mass is apparently enough to cause the large variations observed in the natural frequency and magnitude of this mode. It is unclear why the shaft-bending mode splits into two distinct peaks when the additional 200 lb of lead weights are added on top of the vertical shake plate, but possibilities are discussed later in this section.

A simplified calculation was made using Rayleigh's Method (ref. 10) to help determine how the natural frequency of a shaft-bending mode might vary with hub mass. In making these calculations, the upper and lower bearings on the rotor shaft were assumed to form rigid constraints, and a quadratic mode shape was assumed. The resulting calculations gave a frequency of 12.6 Hz for a hub weight of 800 lb. When the assumed hub weight was increased to 1,000 lb, the frequency dropped to 11.4 Hz. While not identical to the frequencies observed in the shake test, this result validates the observation that the different hub masses could cause the observed changes in the shaft-bending mode natural frequency.

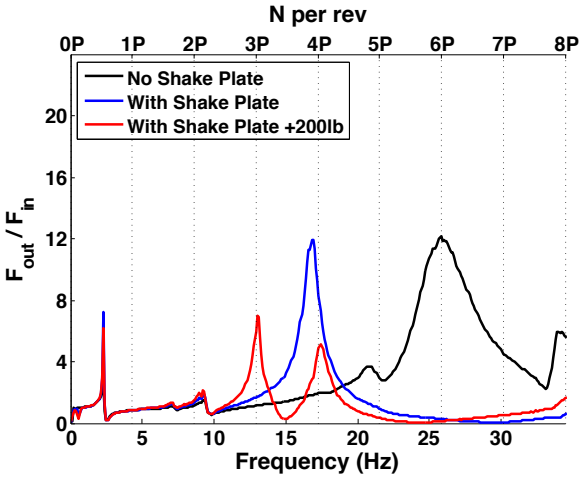

Figure 7. Frequency response magnitude—axial force, 0-deg in-plane shaking.

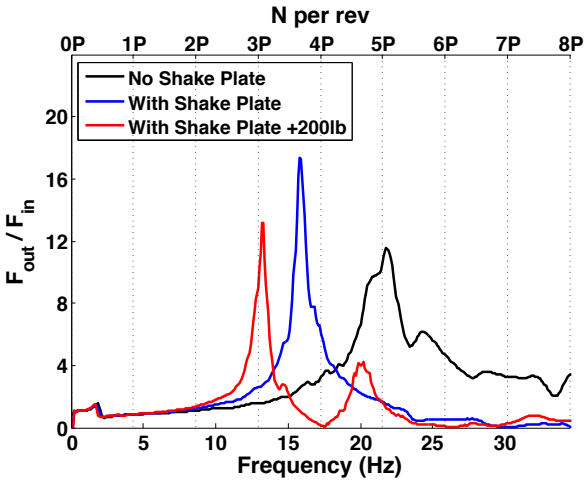

Figure 8. Frequency response magnitude—side force, 270-deg in-plane shaking.

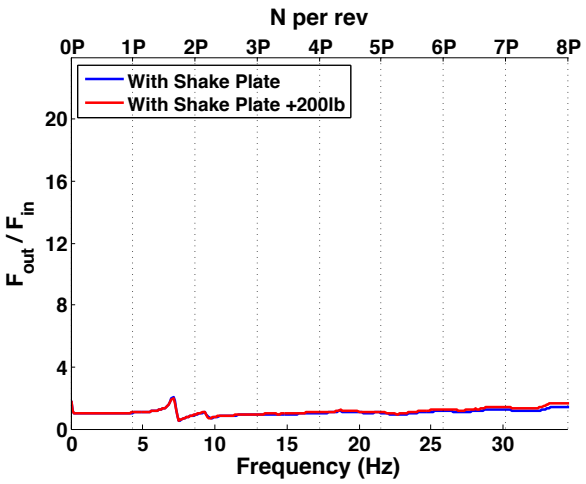

Figure 9. Frequency response magnitude—normal force, vertical on-center shaking.

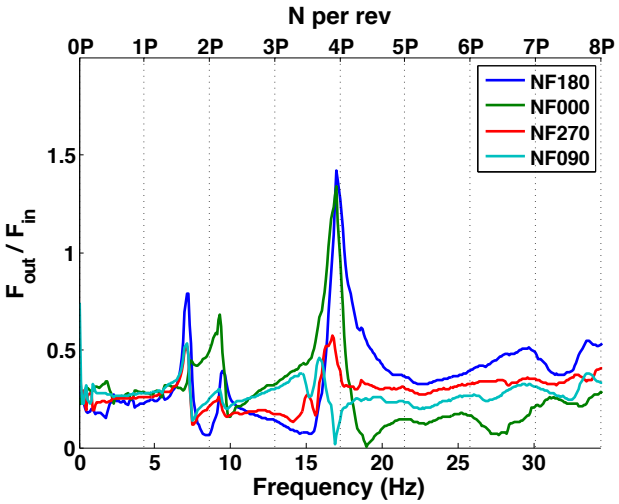

Figure 10. Frequency response magnitude—individual normal force gauge measurements, vertical on-center shaking, shake plate present without additional 200 lb.

In addition to the shaft-bending modes, there are modes that do not change in frequency with hub mass, though they do change in magnitude. The most prominent example of this is the strong axial mode at 2.3 Hz. This is a known mode that is due to bending of the wind tunnel model support struts. There are two additional modes at 7.1 and 9.2 Hz that have not been previously documented. The accelerometer data show that bending of the LRTA chassis is the cause of these modes. The variations observed in the chassis-bending modes appear to be due to superposition with the shaft-bending mode, rather than a global change in the mode shape. The magnitude of the strut-bending mode also varies between hub configurations, but the peak in the FRF is so sharp that this discrepancy is likely due to the frequency resolution of 0.1 Hz. The variations in the FRFs below 1 Hz appear to be artifacts of the signal analysis.

In Figure 9, the response of the LRTA to vertical shaking shows minimal variation with changes in hub mass. There are only two mass configurations for normal force, because the vertical shake plate is necessary to apply loads in the z-direction. The response in the z-direction is mostly flat, with the only observable modes at 7.1 and 9.2 Hz due to chassis bending. Hub mass has little to no effect on the total normal force frequency response, but the shaft-bending mode can, in fact, be excited by normal force excitation. Figure 10 shows the response of the individual normal force gauges to vertical shaking on the hub axis. The forward-aft shaft-bending mode is present here, but the gauge normal forces for this mode are 180 deg out of phase, so they cancel out upon summation.

Cross-coupling with the shaft-bending mode is also visible for in-plane loads between the x- and y-directions. Figure 11a shows the results for in-plane shaking in the axial direction, with response magnitude for both side and axial force. The blue line shows the same data as the blue line in Figure 7: the axial force magnitude from axial shaking. The green line shows the response in the y-direction due to axial shaking. If there were no cross-coupling between side and axial forces, and the experiment was executed perfectly (perfect alignment of the shake direction and 0-deg azimuth), the side force response would be zero; however, near the resonant frequency of the shaft-bending mode, the output side force is nearly three times the input axial force. This result indicates that near the natural frequency of the shaft-bending mode, either the side and axial forces are strongly coupled, or the shaker was not perfectly aligned during the test.

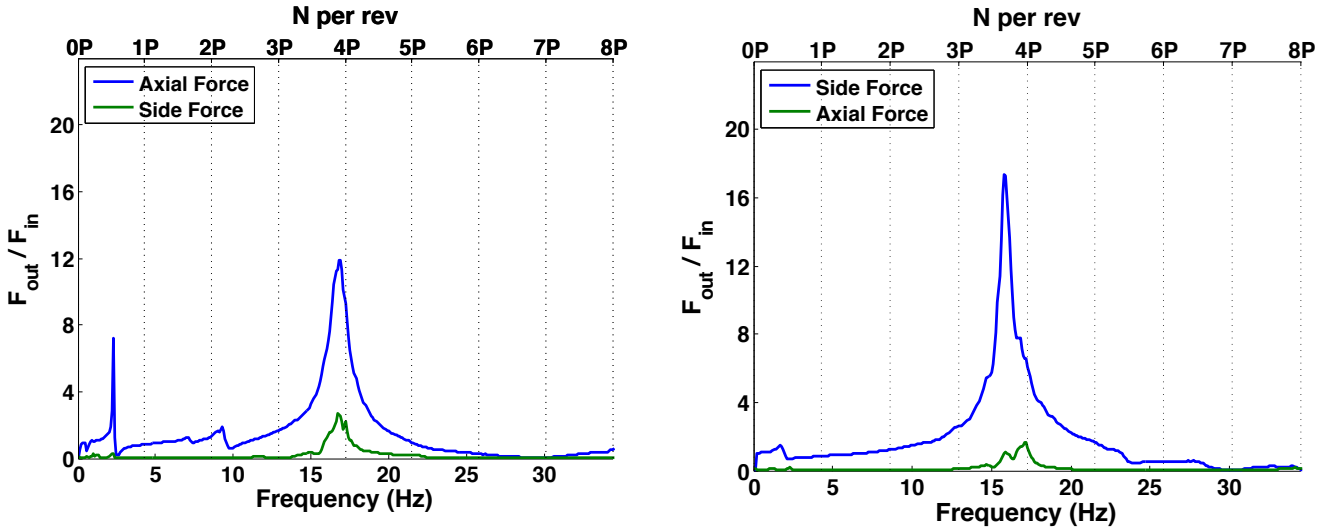

(a) 0-deg in-plane shaking **(b) 270-deg in-plane shaking**

Figure 11. Frequency response magnitude—axial and side force, shake plate present without additional 200 lb.

Figure 11b shows similar results to Figure 11a, except the results in Figure 11b are for in-plane shaking at 270-deg azimuth. The blue line shows the same side force data as the blue line in Figure 8. The green line shows the axial response to the input side force. The apparent cross-coupling is not quite as prominent here as in Figure 11a, but is still present, further indicating that side and axial response may not be independent.

Effect of Angle of Attack

Another independent variable investigated during the shake test was angle of attack. All shake runs except for one were performed at 0-deg alpha, with a single run at 10-deg nose down and shaking applied at 270-deg azimuth. The results are shown in Figure 12. The blue curve is the same as the blue curve in Figure 8. The green curve shows the magnitude of the frequency response for $\alpha = -10$ deg.

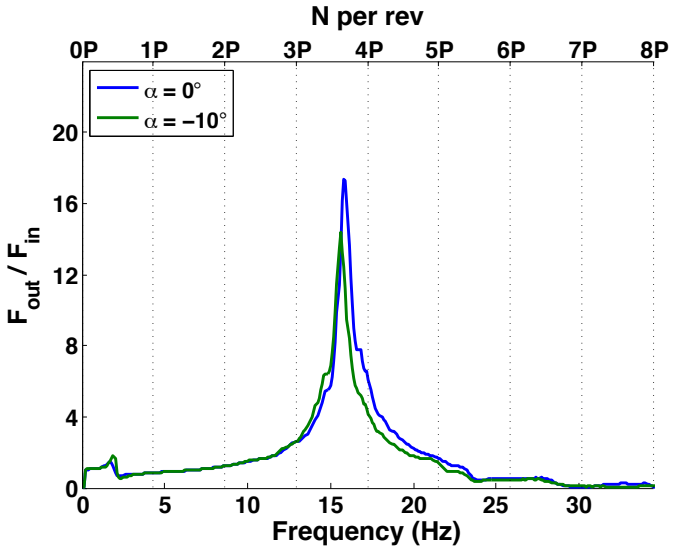

Figure 12. Frequency response magnitude—side force for 270-deg in-plane shaking at varied angle of attack, shake plate present without additional 200 lb.

Angle of attack has almost no effect on the frequency response, except near the shaft-bending mode, where the frequency of the peak differs by 0.2 Hz, and the amplification factor differs by approximately 20 percent. Because there was only a single run at $\alpha = -10$ deg, it is difficult to draw definitive conclusions from the results shown in Figure 12. The plot suggests that angle of attack has only a minor impact on the frequency response in the y-direction, especially compared with FRF changes due to variations in hub mass. The effect on the other two force directions and on moments is unknown. Results from the current NASTRAN model of the LRTA suggest that angle of attack could have a greater impact in the other shake directions, but this effect has not been experimentally verified.

Effect of Shake Direction

For each of the principal axis directions (axial, side, and normal), multiple shake runs can be compared to see how the shake angle affects the response. Figure 13 shows the response in the axial direction for three different shake directions: 0, 50, and 315 deg. Data for the configurations with the shake plate installed both with and without the additional 200 lb are shown. The data for shaking at 50- and 315-deg azimuth are normalized by the input force component in the axial direction, so if the response is independent of shake direction, agreement between the plotted curves for a given hub configuration would be expected.

For both hub configurations, there is very good agreement between shake directions for frequencies between 1 and 12 Hz. For the configuration without the additional mass, the agreement across the entire plotted range is excellent between 0- and 315-deg shaking. The data for 50-deg shaking show a slightly reduced frequency of the mode near 4/rev, and a small split appears in the peak. With the additional 200 lb added to the shake plate, the agreement is not nearly as good. The split peak first shown in Figure 7 for 0-deg shaking is replaced by a single peak for 315-deg shaking. Agreement between 50- and 315-deg shake data is similar to that shown for the case without the additional 200-lb mass.

Similar comparisons can be made for side force and are shown in Figure 14. Zero-deg shaking here is replaced by 270-deg shaking. The agreement here is better than for the axial direction. The results without the additional mass on the shake plate show good agreement for all three shake directions, but 50-deg shaking results in a slightly lower frequency for the main peak in the FRF. There is still a split peak for shaking at 270 deg, but the higher-frequency peak is much less pronounced. Again, the two peaks become a single peak for off-axis shaking.

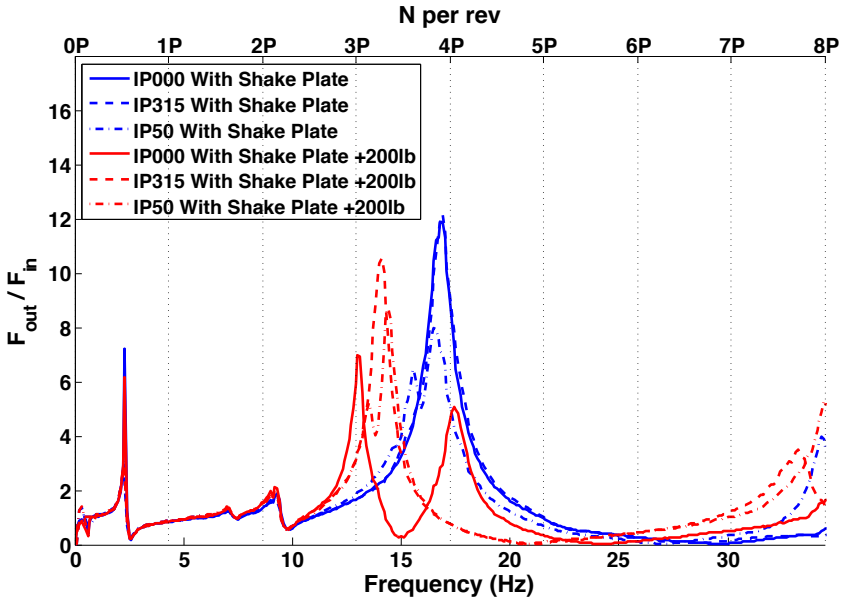

Figure 13. Comparison of in-plane shaking results for axial force response.

It is surprising that the second peak completely disappears for both axial and side force shaking, and this raises the possibility that experimental error played a role. The procedure for the shake test involved leaving the 200 lb of lead weights on the shake plate when the hub was rotated for the next shake direction. Because 270-deg shaking was performed directly after 0-deg shaking, the weights were never removed between shaking in these two directions. It is possible that the weights were installed improperly or there was some other undetected issue that caused the LRTA response to include the double peak shown in Figures 13 and 14. As shown later in Figure 21, the shaft bending gauge results match the balance results very well for 0-deg in-plane shaking with the additional 200 lb, eliminating the possibility of an instrumentation problem causing the double peak.

Results for the four different vertical shake runs can be compared to show the effect of the shake application location on the vertical response. Figure 15 shows the normal force response for all of the vertical shake locations; note that the scale on the ordinate is much smaller than for in-plane shaking, so the differences shown here for vertical shaking are much smaller than for in-plane. The first mode at 7.2 Hz shows excellent agreement between all shake locations for both hub masses. For the mode at 9.3 Hz, it appears that the pitching moment imparted on the chassis for shaking at 0 and 315 deg adds more energy to the mode than on-axis shaking does, generating a stronger response. Between approximately 12 and 18 Hz, the presence of the shaft-bending modes causes variations in the normal force response of up to 50 percent.

Pitch and Roll Moments

Dynamic hub moments were applied by off-center vertical shaking, and the pitching and rolling moment responses are shown in Figures 16a and b, respectively. The moments here are expressed in the balance axes. Once again, the shaft-bending mode dominates the balance-measured response near the 4/rev frequency. The modes below 5 Hz present in Figures 7 and 8 do not appear in the moment measurements. When the additional 200 lb on the vertical shake plate are not present, the frequencies of the modes near 4/rev are identical to those shown in Figures 7 and 8. When the additional weight is added to the shake plate, the frequencies do not match the in-plane results. The double peaks near 3/rev and 4/rev, shown by the red curves in Figures 7 and 8, are replaced by single peaks. The frequencies of the peaks in the pitching and bending moment response plots are similar to the off-primary-axis results shown in Figures 13 and 14.

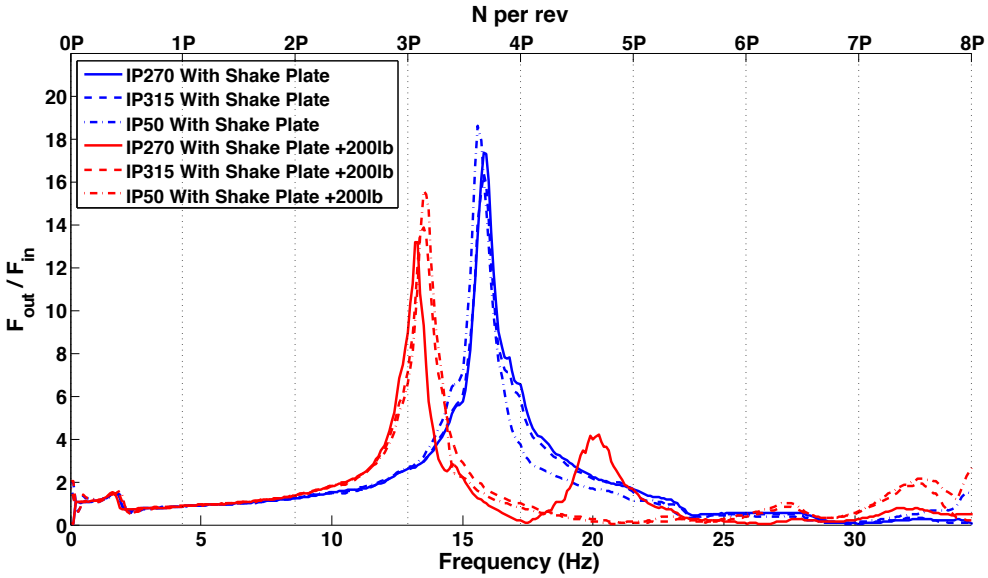

Figure 14. Comparison of in-plane shaking results for side force response.

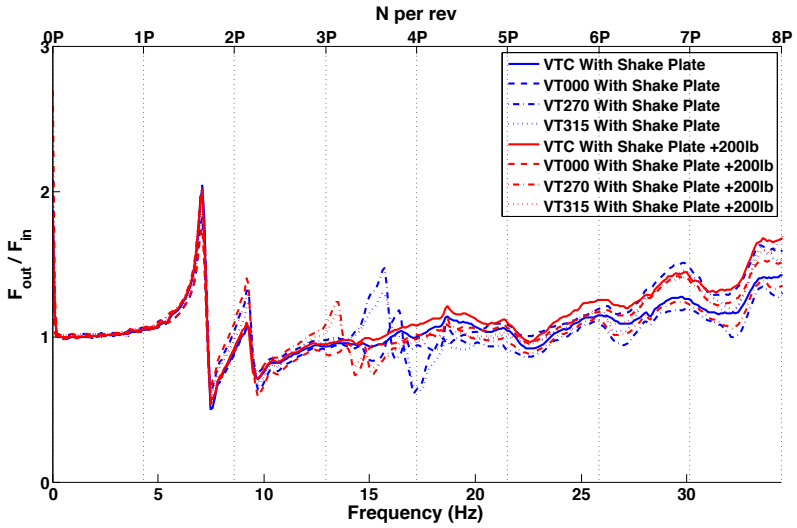

Figure 15. Comparison of vertical shaking results for normal force response.

There were three off-axis vertical shake runs, so the effect of shake location on rolling and pitching moment response can also be investigated. Figures 16a and b show the effect of shake location on the pitch and roll measurements at the balance. There is very little difference in the pitching moment response for the two different shake locations. For roll moment, the agreement is very good below the mast-bending mode frequency. Above it, the difference in response magnitude for the different shake locations appears to be small, but is actually rather large; this isn't immediately evident in the plot, because the magnitude of the shaft-bending peak is so large.

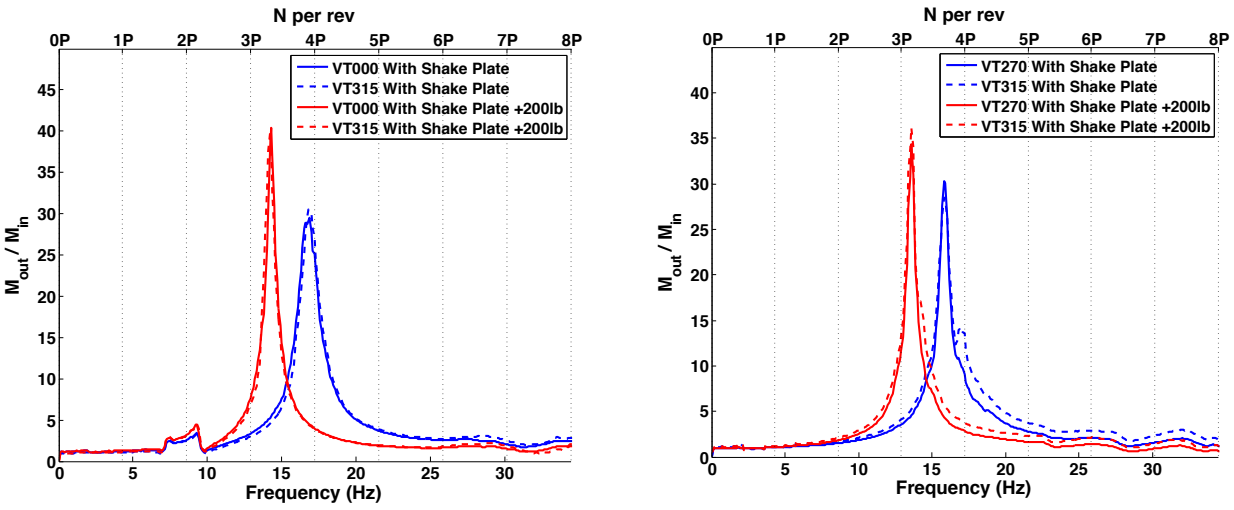

(a) Pitching moment **(b) Rolling moment**

Figure 16. Effect of shake location on pitching and rolling moments measured in the balance axes.

Because in-plane shaking was applied 7.3 inches above the rotor plane at the bifilar, both the in-plane and vertical shake directions generated moments at the hub. Figure 17 shows how the direction of shake application affects the pitching moment response measured by the balance. The plot on the right shows the response measured at the hub if a simple transformation matrix, given in Eq. 2, is used to translate balance loads into the hub axes. In this case, both M_{out} and M_{in} are in the hub axes.

$$\begin{bmatrix} F_x \\ F_y \\ F_z \\ M_x \\ M_y \end{bmatrix}_{hub} = \begin{bmatrix} 1 & 0 & 0 & 0 & 0 \\ 0 & 1 & 0 & 0 & 0 \\ 0 & 0 & 1 & 0 & 0 \\ 0 & -5.12 & 0 & 1 & 0 \\ -5.12 & 0 & 0 & 0 & 1 \end{bmatrix} \begin{bmatrix} F_x \\ F_y \\ F_z \\ M_x \\ M_y \end{bmatrix}_{balance} \tag{2}$$

For all frequencies, Figure 17b shows large differences between the responses generated by in-plane versus vertical shaking. Figure 17a shows the response measured at the balance, with both M_{out} and M_{in} in the balance axes. In this case, there are still differences in the shaft bending mode(s) near 4/rev, but the lower frequency response, which is mostly uniform and unamplified, shows much better agreement.

Two conclusions can be reached from the data shown in Figure 17. First, the simple transformation matrix used to translate static loads from the balance to the hub is insufficient to generate dynamic hub loads from the balance data. Instead, balance moments and in-plane forces will need to be combined with a frequency-dependent calibration matrix to generate moments at the hub. The second conclusion, drawn from Figure 17a, is that the moment response measured at the balance is heavily influenced by the shake direction near the shaft-bending mode and, to a lesser extent, near the two chassis-bending modes. A transfer function based on a single shake direction will therefore be insufficient to calculate hub moments at these frequencies.

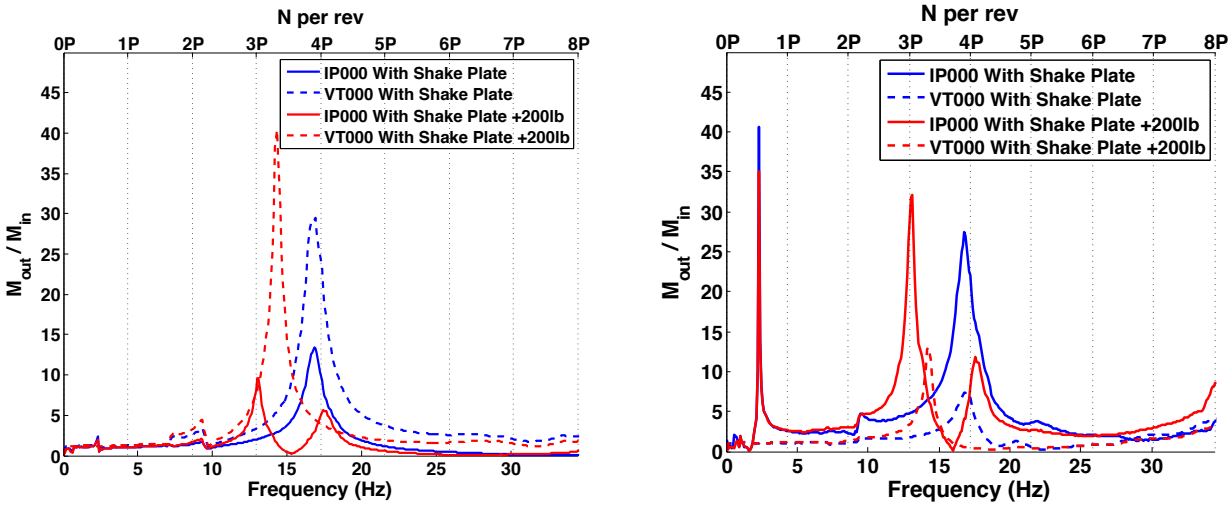

(a) Balance axes **(b) Hub axes**

Figure 17. Effect of shake direction on pitching moment measured in balance axes and hub axes.

Shaft Bending Gauge Results

The shaft bending gauges provided a basis of comparison for the frequency response functions calculated for the balance. Data for the individual bending gauges were recorded during the test and converted to hub forces and moments in post-processing. The formulae used to resolve these forces and moments are the same as those used for the UH-60A Airloads wind tunnel test data, and are given in Appendix A. Sample results for the individual gauges are shown in Figure 18. These results are for in-plane and vertical shaking at 0-deg azimuth. Comparing the bending gauge results in Figure 18 with the balance gauge results in Figure 6, the bending gauges show similar data quality. For the in-plane results shown in Figure 18a, the coherence is close to 1 over most of the frequency range. There is a small dip near the peak at 17 Hz, and a larger drop above 40 Hz where the response is very small. There is 60-Hz noise present in some of the measurements, as shown by the blip in the frequency response and the sharp drop in coherence at that frequency; 60-Hz noise was observed for several of the accelerometers as well.

Unsurprisingly, as was the case with the balance gauges, the coherence for the bending gauges is degraded when the gauges measure a weak response. When the hub is rotated near 0-deg azimuth, as it was for all of the vertical shake runs, the primary bending gauges are located at approximately 0 deg, and the backup gauges are located at approximately 90 deg. The primary bending gauge response is therefore very small for 270-deg shaking, and the backup bending gauge response is very small for 0-deg shaking. Figure 18b shows the bending gauge results for vertical shaking at 0 deg. For the primary gauges, there is a strong response, with good coherence. For the backup gauges, the response is much weaker, and the coherence is not quite as good.

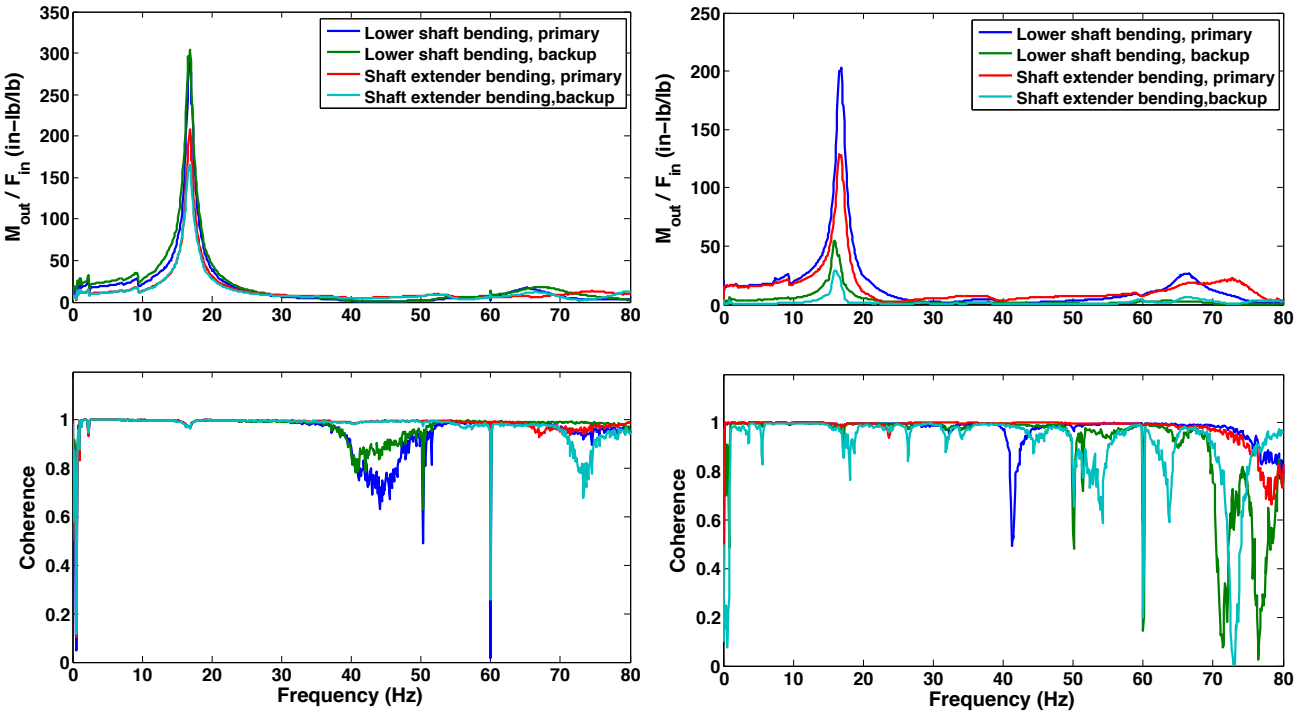

(a) 0-deg in-plane shaking **(b) 0-deg vertical shaking**

Figure 18. Bending gauge results for in-plane and vertical shaking; no additional mass on shake plate.

The individual measurements provided by the four shaft bending gauges were combined to calculate FRFs for in-plane forces and hub pitch and roll moment. Data for the shaft bending gauges were then compared against the results from the balance. There is an assumption here that the equations used to generate static loads from the shaft bending gauges are valid for dynamic loads. Figures 19–21 show the balance and shaft bending gauge axial force with the three different hub configurations for 0-deg in-plane shaking. The blue curves in Figures 19–21 show the same balance data as the black, blue, and red curves, respectively, in Figure 7. The red curves in Figures 19–21 show the corresponding results from the shaft bending gauges. In general, the balance results show good agreement with the shaft bending gauge results, especially for the shaft-bending mode. The agreement improves when the hub mass is higher. For the modes involving the entire LRTA chassis (modes near 2, 7, and 9 Hz), the shaft bending gauges show a small response, but it is weaker than the response measured by the balance.

Pitching and rolling moment frequency response functions for the bending gauges are shown in Figures 22 and 23, expressed in the hub axes. These results are not compared against the balance results here, because, as previously discussed, there is not a simple way to translate the balance pitch and roll moment response functions to the hub axes. The shaft bending gauge results show peaks at the same locations as the balance results shown in Figure 16.

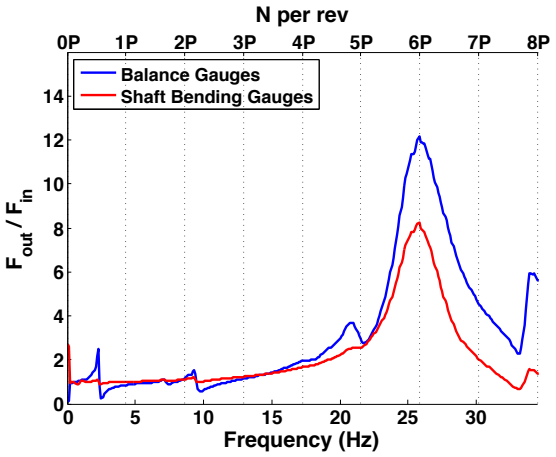

Figure 19. Comparing balance and bending gauges—axial force for 0-deg in-plane shaking, no vertical shake plate.

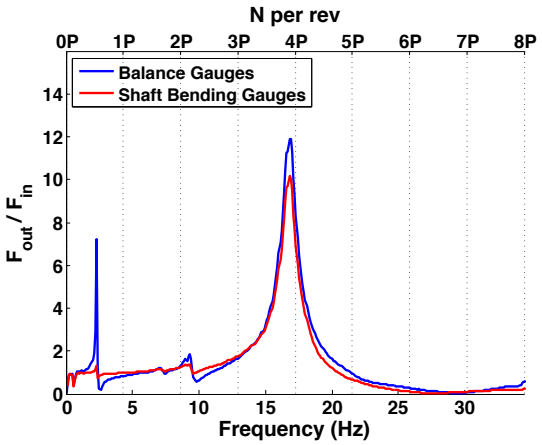

Figure 20. Comparing balance and bending gauges—axial force for 0-deg in-plane shaking, vertical shake plate present without additional mass.

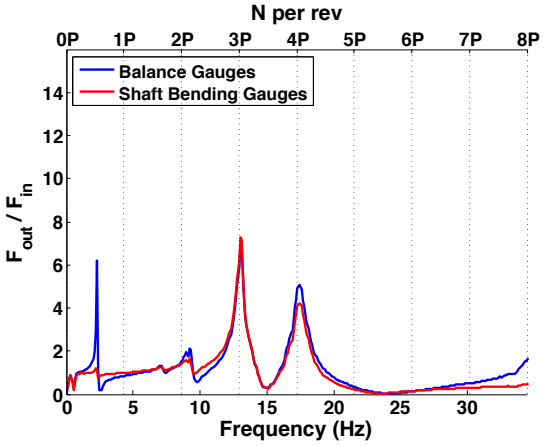

Figure 21. Comparing balance and bending gauges—axial force for 0-deg in-plane shaking, vertical shake plate present with additional 200 lb.

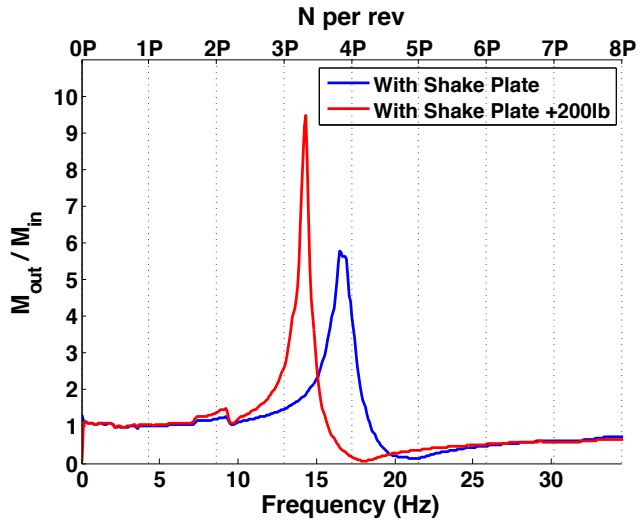

Figure 22. Bending gauge pitching moment for vertical shaking at 0 deg (hub axes).

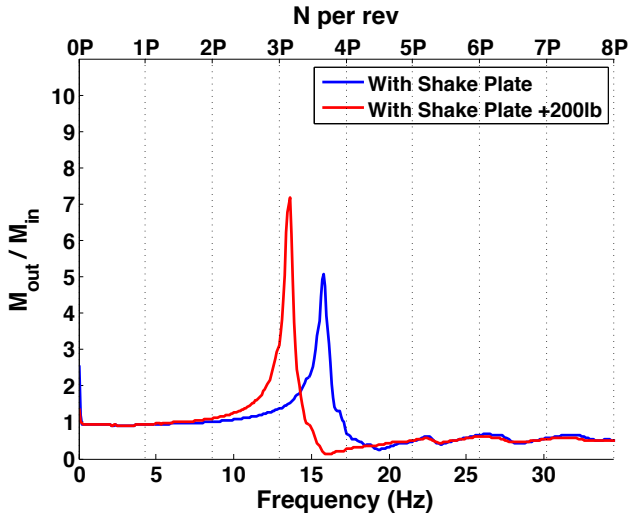

Figure 23. Bending gauge rolling moment for vertical shaking at 270 deg (hub axes).

Insights From the Balance and Bending Gauge Results

The results presented in the previous two sections show that changes in hub mass have a large effect on measurements of in-plane forces and pitch and roll moments on the LRTA. Normal force is largely unaffected by changes in hub mass. The ultimate goal of the shake test described here was a dynamic calibration of the LRTA balance. In order to generate this dynamic calibration, it is necessary to know the amplification factor for the frequency of interest. For the UH-60A, 4/rev is particularly important, but all of the frequencies at the 1/rev through 8/rev harmonics are of interest. The direction of shaking does not have a major impact on force measurement at the balance; however, pitch and roll moments are sensitive to the shake direction, especially near the shaft- and chassis-bending modes. This result indicates that a transfer function calculated from the data for a single shaking direction will not be sufficient to generate a dynamic calibration of the balance. Instead, a multi-dimensional transfer function matrix, calculated from data for multiple shaking directions, will be required to include the effects of off-axis loading.

Based on the results already presented, it would be exceedingly difficult, if not impossible, to create an accurate calibration over the entire frequency range of interest with the shake test data alone. The peaks in the FRFs are very narrow, so a natural frequency change of even 0.5 Hz could easily change the amplification by a factor of two or more. The presence of a shaft-bending mode that is both near the 4/rev frequency and is highly dependent on hub mass is problematic.

Accelerometer Results

Frequency response and coherence data for the accelerometers are tabulated in Appendix C, but some samples of the accelerometer data are given here. The accelerometer data show a large range of response magnitude and coherence, depending on the direction and location of the measurement. Figure 24a shows the response at the hub instrumentation hat in the axial direction for 0-deg in-plane shaking. Figure 24b shows the results for the same test run, but for the vertical acceleration at the instrumentation hat. Figure 25 also shows results for 0-deg in-plane shaking, but for an accelerometer located at the forward end of the LRTA chassis.

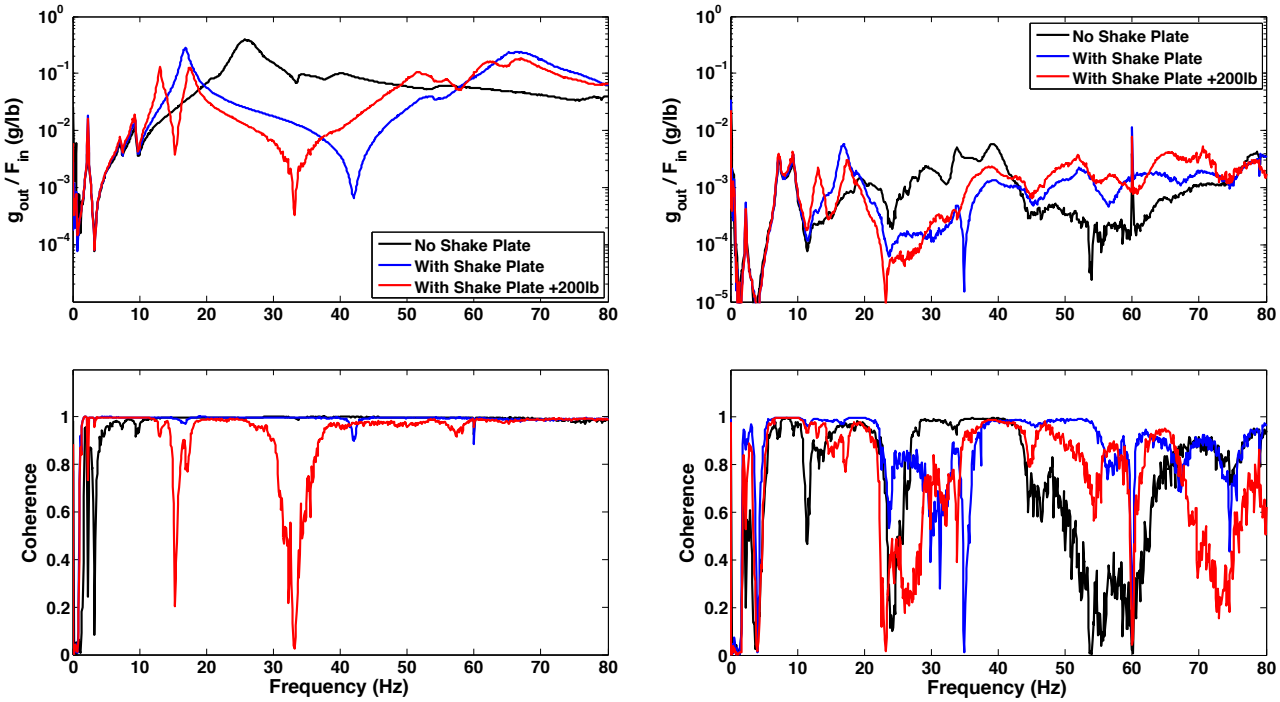

(a) x-direction (b) z-direction

Figure 24. Instrumentation hat accelerometer results for 0-deg in-plane shaking.

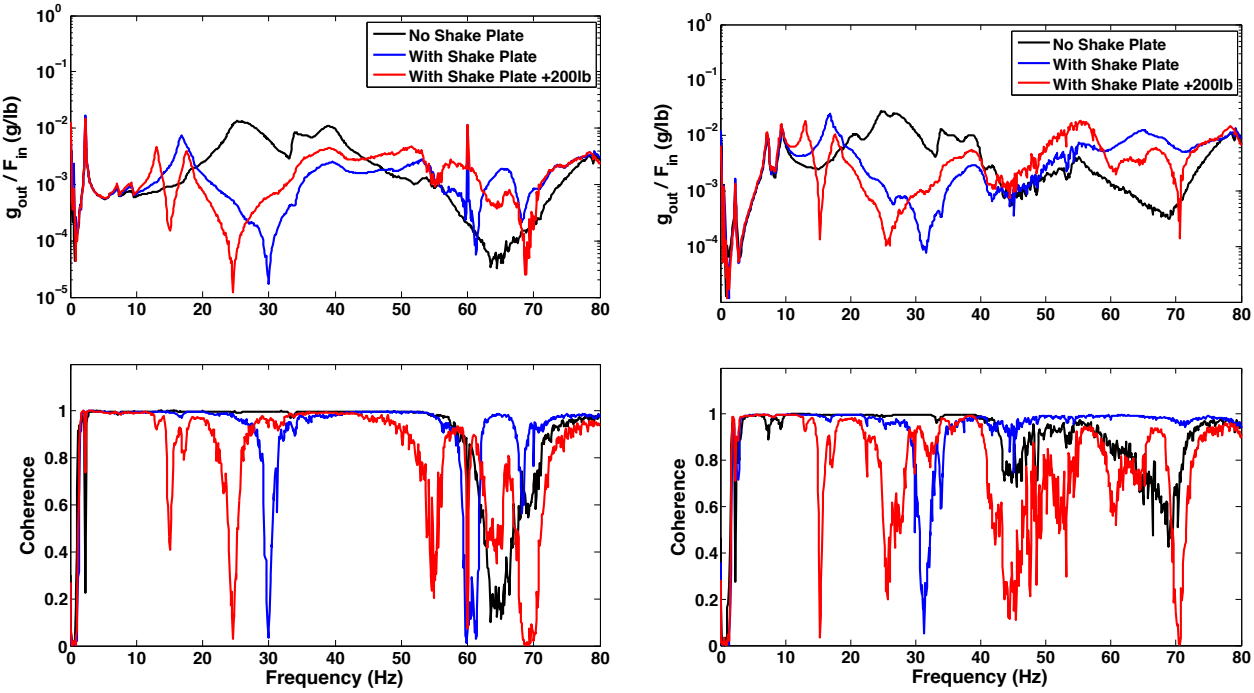

(a) x-direction (b) z-direction

Figure 25. LRTA forward end accelerometer results for 0-deg in-plane shaking.

There are several observations to be made from the accelerometer data in Figures 24 and 25:

- The mode that changes frequency with hub mass is indeed due to shaft bending; the response in the x-direction at the instrumentation hat is at least an order of magnitude greater than the response in the other directions and location shown.
- The modes observed at 2.3, 7.2, and 9.3 Hz are more global modes. The 2.3-Hz strut-bending mode shows a similar magnitude at both the instrumentation hat and the forward end of the chassis in the x-direction. The modes at 7.2 and 9.3 Hz show similar magnitudes at both locations in the z-direction.
- Compared with the balance and bending gauge results, the coherence for the accelerometers shows larger dips coincident with the peaks in the FRFs, indicating greater uncertainty in the magnitude of those peaks.
- The coherence is rather poor below approximately 3 Hz, which affects the measurements of the strut-bending mode at 2.3 Hz.
- Above approximately 40 Hz, the FRFs are jagged, and the coherence is poor, indicating that the shaker was adding insufficient energy to the system at higher frequencies to excite the entire LRTA. In general, only the x- and y-direction accelerometers on the rotor shaft show smooth transfer functions with high coherence above 40 Hz.
- The instrumentation hat accelerometer shows a rounded peak near 70 Hz, but only for the cases where the shake plate is present. This mode is discussed in the following section.

An easier way to interpret the mode shapes is to draw them using data for all of the accelerometers at once. Figure 26a shows an exaggerated drawing of the mode shape at 7.2 Hz. The data used to generate this drawing are from 0-deg in-plane shaking with the vertical shake plate present and without the additional 200 lb of lead weights. It is clear from the drawing that this particular mode involves the entire LRTA chassis and the support struts. Figure 27a shows a similar drawing for the mode at 16.9 Hz for the same test condition, and it is clear that this mode is dominated by bending of the rotor shaft. Note that the scale for the drawing of the chassis-bending mode is 10 times that of the shaft-bending mode, because the shaft-bending mode has a much stronger response.

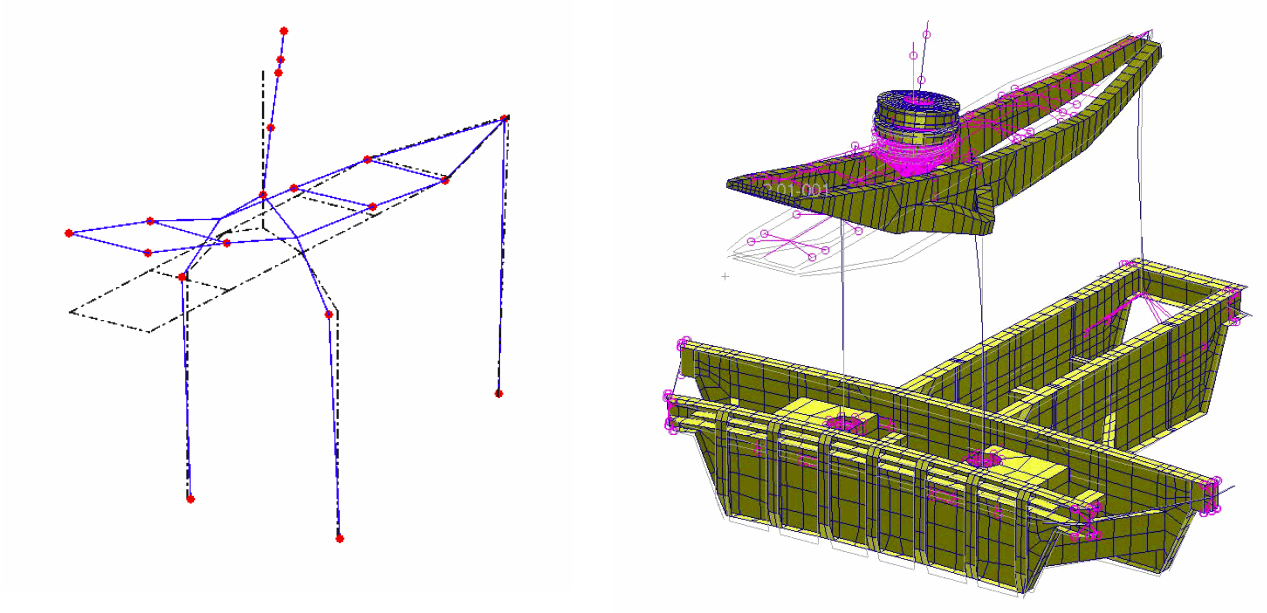

(a) Accelerometer data (scale 10^7)—7.2 Hz **(b) NASTRAN prediction—8.9 Hz**

Figure 26. Comparison of accelerometer data and NASTRAN model—Mode 3.

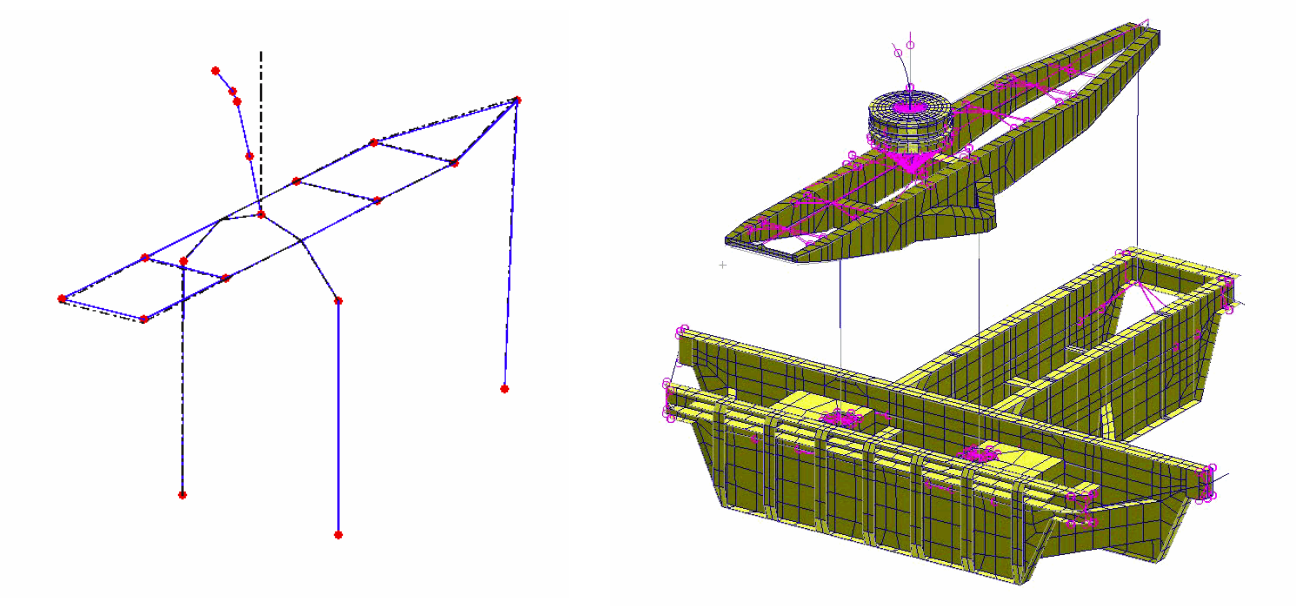

(a) Accelerometer data (scale 10^6)—16.9 Hz **(b) NASTRAN prediction—29.9 Hz**

Figure 27. Comparison of accelerometer data and NASTRAN model—Mode 6.

One approach that has been proposed for generating a dynamic calibration is to create a finite element analysis (FEA) model that can be tuned to replicate the behavior of the LRTA. Transfer functions would then be generated based on simulation results. Accelerometer mode shape and frequency data were used to compare the experimental results of the shake test with results from an existing NASTRAN model. This NASTRAN model includes the LRTA chassis, balance, support struts, and T-frame base. Six of the modes identified by analysis of the NASTRAN model are clearly visible in the shake test data.

The modes that are recognizable in both the NASTRAN model and the accelerometer data are identified in Table 2. Figures 26 and 27 show comparisons between the accelerometer mode shape (a) and the corresponding NASTRAN mode shape (b) for mode numbers 3 and 6 listed in Table 2. Images of the other four mode shapes are contained in Appendix B in Figures B1 to B4. The red dots on the left-hand image indicate the locations of the accelerometers. The dotted or gray lines in both images show the un-deformed shape of the LRTA. The large T-shaped frame shown in Figures 26b and 27b sits under the turntable of the 40- by 80-foot test section and is the base for the model support struts.

There are some noticeable differences between the predicted and measured mode shapes, particularly for the lateral modes. While it is not obvious from Figure B1, the measured mode shape for Mode 1, lateral strut bending, shows significantly more torsion of the entire LRTA chassis about a vertical axis than the matching NASTRAN mode shape. There is, however, a second strut bending mode predicted by the NASTRAN model involving only torsion about a vertical axis, so the observed mode shape is likely a combination of two of the predicted modes. For Mode 5, lateral rotor shaft bending (Fig. B4), the NASTRAN model predicts much more bending of the LRTA chassis than was observed.

Even though the mode shapes are similar, the frequencies are not identical. In general, the NASTRAN model over-predicts the frequency, and the amount of over-prediction increases with the frequency of the mode. The shake test frequencies in Table 2 are for the case where the vertical shake plate is present, but the additional 200 lb of lead weights are not. The balance force FRFs for the three principle shake directions are shown in Figure 28 with the Table 2 mode numbers identified in red.

Table 2. Modes and frequencies from both the NASTRAN model and the shake test.

Mode Number	Mode Shape	NASTRAN Frequency (Hz)	Shake Test Frequency (Hz)
1	Lateral strut bending	2.4	1.7
2	Longitudinal strut bending	2.4	2.3
3	Chassis vertical bending	8.9	7.2
4	Chassis + T-frame vertical bending	13.4	9.3
5	Rotor shaft lateral bending	26.1	15.9
6	Rotor shaft longitudinal bending	29.9	16.9

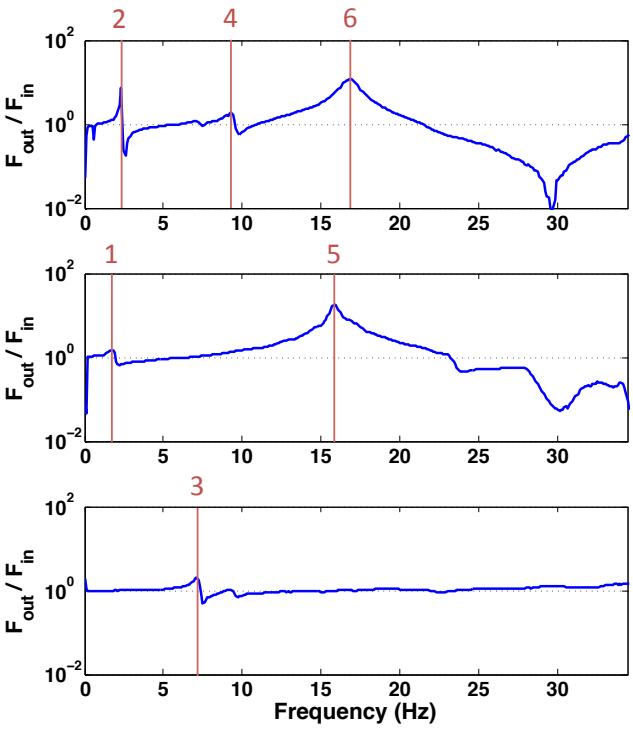

Figure 28. Mode identification for axial force, in-plane shaking at 0 deg (top); side force, in-plane shaking at 270 deg (middle); normal force, vertical shaking on-center (bottom). Note logarithmic scale on y-axis.

The NASTRAN model has not been tuned to match the accelerometer data, but the fact that several of the mode shapes approximately match is encouraging. To explore whether an FEA model of the LRTA could be tuned to match the behavior of the test rig, a 3-dimensional solid model was developed using the Creo mechanical design software suite (ref. 11). Because the shaft-bending modes involve very little motion of the LRTA chassis, a simplified FEA model was used, including just the LRTA output shaft and UH-60A shaft extender. The hub was modeled as a point mass. Changing the mass at the hub as well as adjusting the height of the hub above the top of the output shaft had a large effect on the first natural frequency calculated by the FEA model. This result indicates that it would be possible to tune the FEA model to match the behavior of the LRTA; however, a calibration has not yet been generated using this method. This is a possible avenue for future research.

It may also be possible to directly measure rotor loads with accelerometer data. This method is detailed in reference 12, and relies on measuring the vibratory response of an entire airframe to applied loads. To measure rotor loads, the method would require placing accelerometers on the LRTA during wind tunnel testing, which was not the case for the Airloads wind tunnel test. With the accelerometer data already collected, though, this method could be useful for future wind tunnel tests.

Vertical Shake Plate Impacts

As previously noted in accelerometer data shown in Figure 24a, there is a weak mode that appears near 70 Hz. A further look at the accelerometer data reveals that this mode is due to in-plane vibration of the vertical shake plate. Figure 29 shows the accelerometer mode shape at 67.0 Hz for 0-deg in-plane shaking with the vertical shake plate (no additional lead weights). The topmost red dot in Figure 29 represents the accelerometer mounted on the vertical shake plate. At 67.0 Hz, there is some motion of the rotor shaft, but the mode shape is clearly defined by horizontal motion of the shake plate. This means that the shake plate could actually be acting as a vibration absorber in this frequency range, which would make the higher-frequency shake test results less reliable.

A brief rap test was performed on the shake plate while it was installed on the rotor hub. The purpose of this rap test was to evaluate whether a hammer impact could provide sufficient excitation of the LRTA to generate the same mode shapes as the shake test. If it is indeed possible to provide sufficient input energy with a hammer impact, future vibration testing could be vastly simplified by eliminating the need for the shaker system and suspended reaction mass. A single 50-g triaxial accelerometer was used to measure the response. Figure 30 shows a comparison of the rap test and shake test results; both curves show the axial response for 0-deg excitation. The full set of rap test data is contained in Appendix C, and the accelerometer and rap directions are listed in Table A4 in Appendix A; three of the rap test directions are aligned with shake test directions. The rap hammer was able to excite the shaft-bending mode and the vertical shake plate mode, but it does not appear that any other mode of the LRTA was excited. This indicates that the rap hammer did not provide enough energy to the system to excite the LRTA chassis modes. A rap test could therefore be useful for determining the natural frequency of the shaft-bending mode, but not for dynamic characterization of the entire LRTA.

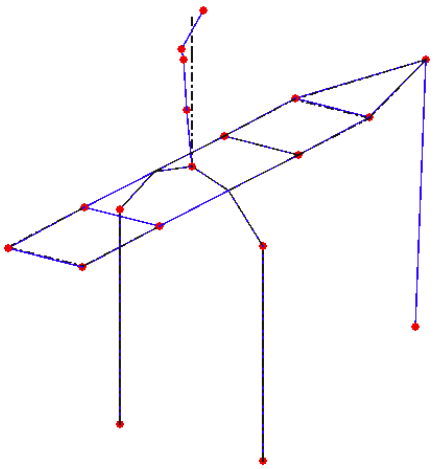

Figure 29. Accelerometer results for 0-deg in-plane shaking at 67.0 Hz.

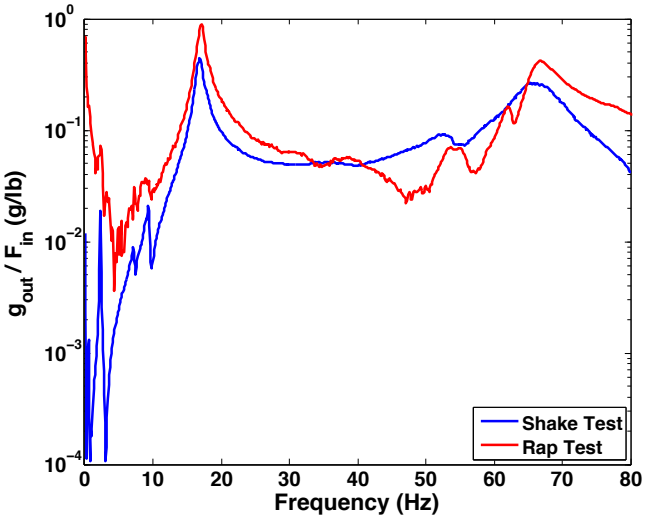

Figure 30. Comparison of rap test and shake test results for the vertical shake plate.

CONCLUSIONS

This paper presented the results of a shake test of the Large Rotor Test Apparatus, carried out in the 40- by 80-foot test section of the National Full-Scale Aerodynamics Complex. This test was executed prior to the UH-60A Airloads wind tunnel test with the intention of generating a dynamic calibration of the LRTA five-component rotor balance. Frequency response data were collected for the balance as well as the shaft bending gauges and for accelerometers placed on the LRTA. Sample results were evaluated here. Based on the results presented, the following conclusions can be drawn:

1. The shake test provided a large set of frequency response data for the LRTA for a variety of hub loading scenarios at frequencies up to 80 Hz. In general, the data look useful for frequencies below approximately 35 Hz, or 8/rev for the UH-60A rotor.

2. The addition of the shake plate that was used to facilitate shaking in the vertical direction represents a significant increase in mass at the hub, which modified the natural frequencies of the LRTA. The vertical shake plate also introduced its own natural frequency at 67 Hz. It would be preferable to perform this type of shake test without adding a large, flexibly attached mass to the hub.

3. At frequencies near 4/rev of the UH-60A rotor (17.2 Hz), the LRTA has a strong shaft-bending mode that is highly dependent on the mass of the hub. The variability of this mode makes determination of moments and in-plane loads at 3/rev (12.9 Hz) and higher difficult, if not impossible, if the dynamic calibration of the balance is based on the shake test data alone.

4. The normal loads measured at the balance are only minimally affected by hub mass. Normal loads up to 7/rev (30.1 Hz) can therefore be corrected based on the shake test balance data.

5. The shaft bending gauges provide another means of measuring dynamic hub loads, but these measurements are also affected by hub mass.

6. Interactions between moments and in-plane forces will require a calibration matrix calculated from multiple loading directions in order to accurately measure hub loads with the balance, especially near natural frequencies of the LRTA.

7. Accelerometer data provided mode shapes that correspond to an existing NASTRAN model of the LRTA. Tuning the NASTRAN model to match the accelerometer data may provide another means of dynamic loads calibration.

RECOMMENDATIONS

The data gathered for this shake test should not be used alone to generate a dynamic calibration of the LRTA balance for the entire frequency range of interest (up to 8/rev for the UH-60A rotor, or 34.4 Hz). There is too much uncertainty in the magnitude of the transfer function from hub to balance. For frequencies below approximately 10 Hz, it may be feasible to correct measured hub loads with a calibration based on the shake test data alone. This could prove particularly useful for correcting dynamic hub loads for slowed-rotor testing, as shown in reference 4.

Additional mathematical modeling will be required to correct dynamic loads above 10 Hz, because of the impact of hub mass on the dynamic response of the LRTA. One approach that was originally proposed as part of this shake test activity is to tune the existing NASTRAN model to match the dynamic response observed during the shake test. With a properly tuned NASTRAN model, loads could be simulated to generate the necessary transfer

functions from the hub to the balance. The existing NASTRAN model has thousands of elements, so properly adjusting it may not be feasible; however, optimization techniques, such as those proposed in reference 8, could provide an efficient means of tuning the NASTRAN model. Alternatively, a simpler FEA model could be developed that could more easily be tuned.

This shake test has highlighted the difficulty that arises when a rotor test stand has a shaft-bending mode in the frequency range of interest. This same issue was observed in the RTA shake test results in reference 5. If possible, when designing a rotor test stand, the natural frequency(s) of the shaft-bending mode should be placed above the frequency range of interest. This may not be feasible because of geometric or material constraints. If the shaft-bending mode (or any other mode strongly affected by hub mass) can be placed outside the frequency range of interest, a much simpler and more accurate dynamic calibration of the balance would be expected.

REFERENCES

1. Harris, F. D.: *Introduction to Autogyros, Helicopters, and other V/STOL Aircraft, Vol. 2: Helicopters*. NASA SP-2012-215959, Vol. 2, Oct. 2012, pp. 315–435.

2. Norman, T.; Shinoda, R.; Kitaplioglu, C.; Jacklin, S.; and Sheikman, A.: Low-Speed Wind Tunnel Investigation of a Full-Scale UH-60 Rotor System. American Helicopter Society 58th Annual Forum, Montreal, Canada, June 11–13, 2002.

3. Norman, T.; Shinoda, P.; Peterson, R.: and Datta, A.: Full-Scale Wind Tunnel Test of the UH-60A Airloads Rotor. American Helicopter Society 67th Annual Forum, Virginia Beach, VA, May 3–5, 2011.

4. Russell, C.: Shake Test Results and Dynamic Calibration Efforts for the Large Rotor Test Apparatus. American Helicopter Society Aeromechanics Specialists Conference, San Francisco, CA, Jan. 22–24, 2014.

5. Peterson, R. and van Aken, J.: Dynamic Calibration of the NASA Ames Rotor Test Apparatus Steady/Dynamic Rotor Balance. NASA TM 110393, Apr. 1996.

6. van Aken, J.; Peterson, R.; and Freedman, C.: Calibration Results of the NASA Ames Rotor Test Apparatus Steady/Dynamic Rotor Balance. American Helicopter Society Aeromechanics Specialists Conference, San Francisco, CA, Jan. 19–21, 1994.

7. Wang, J., and van Aken, J.: Correlation of Vibratory Hub Loads for a Sikorsky Full-Scale Bearingless Main Rotor. American Helicopter Society 50th Annual Forum, Washington, D.C., May 11–13, 1994.

8. Chapleau, S.; Seifert, M.; and Couture, M.: Dynamics FEM Correlation Using Structural Optimization Tools. American Helicopter Society 70th Annual Forum, Montreal, Québec, Canada, May 20–22, 2014.

9. *MSC NASTRAN 2012 Quick Reference Guide*, MSC Software Corp., Newport Beach, CA, 2012.

10. Rao, S.: *Mechanical Vibrations*, Pearson Education, Inc., NJ, 2004, pp. 631–632.

11. *PTC Creo® Simulate Data Sheet*, PTC Inc., Needham, MA, 2012.

12. Giansante, N.; Jones, R.; and Calapodas, N. J.: Determination of In-Flight Helicopter Loads. American Helicopter Society 37th Annual Forum, New Orleans, LA, May 17–20, 1981.

APPENDIX A. INSTRUMENTATION

Table A1. Approximate accelerometer locations (inches).*

NODE	X	Y	Z	NOTE
0	0	0	266	Bifilar
1	0	0	274	Instrumentation hat
2	0	0	189	Balance base
3	0	50	147	Right strut tip
4	–155	26	179	Right frame front end
5	–155	–26	179	Left frame front end
6	0	–50	147	Left strut tip
7	149	26	179	Left frame aft end
8	74	26	179	Right frame mid aft
9	249	0	179	Tail strut tip
10	0	50	0	Right strut base
11	0	–50	0	Left strut base
12	74	–26	179	Left frame mid aft
13	149	–26	179	Right frame aft end
14	238	0	0	Tail strut base
15	–74	26	179	Right frame mid front
16	–74	–26	179	Left frame mid front
17	0	0	229	Mid shaft
18	0	26	179	Right frame mid
19	0	–26	179	Left frame mid
20	0	0	291	Vertical shake plate

* x and y locations are referenced to the hub centerline. z locations are referenced to the base of the struts. Coordinate system is shown in green in Figure A1. Hub center is at (x, y, z) = (0, 0, 258.7) inches.

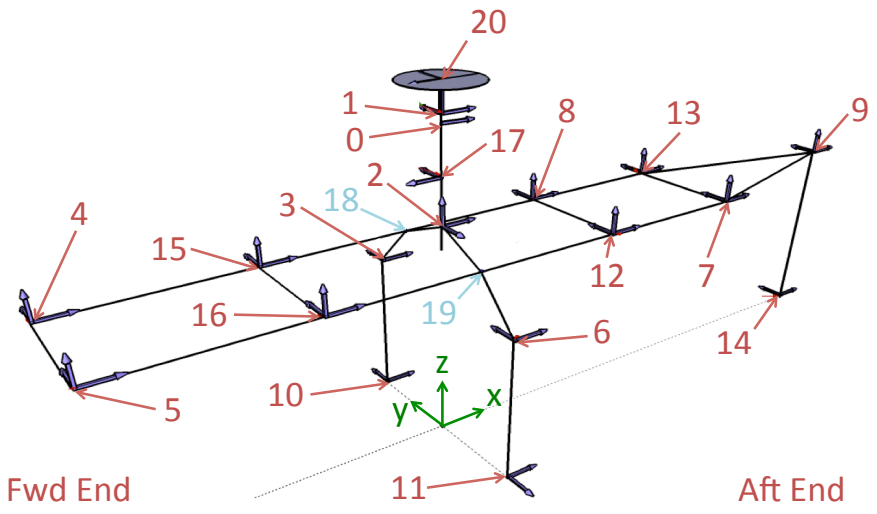

Figure A1. Accelerometer locations and directions. Note that nodes 18 and 19 were not instrumented.

Table A2. Run-by-run accelerometer locations and directions.*

Accel ID	Run 1 - IP000		Run 2 - IP270		Run 3 - IP315		Run 4 - IP50		Run 5 - VTC		Run 6 - VT000		Run 7 - VT270		Run 8 - VT315		Run 9 - IP270A10		Run 10 - IP270NVP		Run 11 - IP000NVP	
	Node	Direction	Node	Direction	Node	Direction	Node	Direction	Node	Direction	Node	Direction	Node	Direction	Node	Direction	Node	Direction	Node	Direction	Node	Direction
acc1	**0**	**180**	**0**	**90**	**0**	**135**	**0**	**230**	**20**	**down**	**20**	**down**	**20**	**down**	**20**	**down**	**0**	**90**	**0**	**90**	**0**	**180**
acc2	**1**	**180**	**1**	**90**	**1**	**135**	**1**	**230**	**1**	**226**	**1**	**226**	**1**	**226**	**1**	**226**	**1**	**90**	**1**	**90**	**1**	**180**
acc3	**1**	**270**	**1**	**180**	**1**	**225**	**1**	**320**	**1**	**316**	**1**	**316**	**1**	**316**	**1**	**316**	**1**	**180**	**1**	**180**	**1**	**270**
acc4	1	up	1	up	1	up	1	up	1	up	1	up	1	up	1	up	1	up	1	up	1	up
acc5	2	0	2	0	2	0	2	0	2	0	2	0	2	0	2	0	2	0	2	0	2	0
acc6	2	270	2	270	2	270	2	270	2	270	2	270	2	270	2	270	2	270	2	270	2	270
acc7	2	up	2	up	2	up	2	up	2	up	2	up	2	up	2	up	2	up	2	up	2	up
acc8	3	0	3	0	3	0	3	0	3	0	3	0	3	0	3	0	3	0	3	0	3	0
acc9	3	90	3	90	3	90	3	90	3	90	3	90	3	90	3	90	3	90	3	90	3	90
acc10	**20**	**0**	**20**	**270**	**20**	**315**	**20**	**50**	**20**	**46**	**20**	**46**	**20**	**46**	**20**	**46**	**20**	**270**	--	--	--	--
acc11	4	0	4	0	4	0	4	0	4	0	4	0	4	0	4	0	4	0	4	0	4	0
acc12	4	90	4	90	4	90	4	90	4	90	4	90	4	90	4	90	4	90	4	90	4	90
acc13	4	up	4	up	4	up	4	up	4	up	4	up	4	up	4	up	4	up	4	up	4	up
acc14	5	0	5	0	5	0	5	0	5	0	5	0	5	0	5	0	5	0	5	0	5	0
acc15	5	90	5	90	5	90	5	90	5	90	5	90	5	90	5	90	5	90	5	90	5	90
acc16	5	up	5	up	5	up	5	up	5	up	5	up	5	up	5	up	5	up	5	up	5	up
acc17	6	0	6	0	6	0	6	0	6	0	6	0	6	0	6	0	6	0	6	0	6	0
acc18	6	90	6	90	6	90	6	90	6	90	6	90	6	90	6	90	6	90	6	90	6	90
acc19	**20**	**270**	**20**	**180**	**20**	**225**	**20**	**320**	**20**	**316**	**20**	**316**	**20**	**316**	**20**	**316**	**20**	**180**	--	--	--	--
acc20	7	0	7	0	7	0	7	0	7	0	7	0	7	0	7	0	7	0	7	0	7	0
acc21	7	90	7	90	7	90	7	90	7	90	7	90	7	90	7	90	7	90	7	90	7	90
acc22	7	up	7	up	7	up	7	up	7	up	7	up	7	up	7	up	7	up	7	up	7	up
acc23	8	0	8	0	8	0	8	0	8	0	8	0	8	0	8	0	8	0	8	0	8	0
acc24	8	90	8	90	8	90	8	90	8	90	8	90	8	90	8	90	8	90	8	90	8	90
acc25	8	up	8	up	8	up	8	up	8	up	8	up	--	--	--	--	8	up	8	up	8	up
acc26	9	0	9	0	9	0	9	0	9	0	9	0	9	0	9	0	9	0	9	0	9	0
acc27	9	90	9	90	9	90	9	90	--	--	9	90	9	90	9	90	9	90	9	90	9	90
acc28	9	up	9	up	9	up	9	up	9	up	9	up	9	up	9	up	9	up	9	up	9	up
acc29	10	0	10	0	10	0	10	0	10	0	10	0	10	0	10	0	10	0	10	0	10	0
acc30	10	90	10	90	10	90	10	90	10	90	10	90	10	90	10	90	10	90	10	90	10	90
acc31	11	0	11	0	11	0	11	0	11	0	11	0	11	0	11	0	11	0	11	0	11	0
acc32	11	270	11	270	11	270	11	270	11	270	11	270	11	270	11	270	11	270	11	270	11	270
acc33	12	0	12	0	12	0	12	0	12	0	12	0	12	0	12	0	12	0	12	0	12	0
acc34	12	90	12	90	12	90	12	90	12	90	12	90	12	90	12	90	12	90	12	90	12	90
acc35	12	up	12	up	12	up	12	up	12	up	12	up	12	up	12	up	12	up	12	up	12	up
acc36	13	0	13	0	13	0	13	0	13	0	13	0	13	0	13	0	13	0	13	0	13	0
acc37	13	90	13	90	13	90	13	90	13	90	13	90	13	90	13	90	13	90	13	90	13	90
acc38	13	up	13	up	13	up	13	up	13	up	13	up	13	up	13	up	13	up	13	up	13	up
acc39	14	0	14	0	14	0	14	0	14	0	14	0	14	0	14	0	14	0	14	0	14	0
acc40	14	90	14	90	14	90	14	90	14	90	14	90	14	90	14	90	14	90	14	90	14	90
acc41	15	0	15	0	15	0	15	0	15	0	15	0	15	0	15	0	15	0	15	0	15	0
acc42	15	90	15	90	15	90	15	90	15	90	15	90	15	90	15	90	15	90	15	90	15	90
acc43	15	up	15	up	15	up	15	up	15	up	15	up	15	up	15	up	15	up	15	up	15	up
acc44	16	0	16	0	16	0	16	0	16	0	16	0	16	0	16	0	16	0	16	0	16	0
acc45	16	90	16	90	16	90	16	90	16	90	16	90	16	90	16	90	16	90	16	90	16	90
acc46	16	up	16	up	16	up	16	up	16	up	16	up	16	up	16	up	16	up	16	up	16	up
acc47	17	90	17	90	17	90	17	90	17	90	17	90	17	90	17	90	17	90	17	90	17	90

*** Entries in bold indicate the accelerometer was either moved or rotated from run to run. A '--' means the accelerometer was not connected or had a dead response.**

Table A3. Run list and instrumentation settings.

Run	Description	Hub Azimuth (deg)	Signal Type	Excitation Frequency (Hz)	Excitation Amplitude (lb)	Window
1	IP000[1]	–49.2	Burst Random	0–80	800	None
	IP000-200[2]	–49.2	Burst Random	0–80	600	None
2	IP270	–139.9	Thump Random	0–80	Undocumented	Undocumented
	IP270-200	–139.9	Thump Random	0–80	Undocumented	Undocumented
3	IP315	–95.1	Thump Random	0–80	400	Hanning Broad
	IP315-200	–95.1	Thump Random	0–80	800	Hanning Broad
4	IP50	0	Thump Random	0–80	600	Hanning Broad
	IP50-200	0	Thump Random	0–80	400	Hanning Broad
5	VTC[3]	–4.31	Pseudo-random	0–100	Undocumented	Hanning Broad
	VTC-200	–4.31	Pseudo-random	0–100	Undocumented	Hanning Broad
6	VT000	–4.31	Pseudo-random	0–100	Undocumented	Hanning Broad
	VT000-200	–4.31	Pseudo-random	0–100	Undocumented	Hanning Broad
7	VT270	–4.31	Pseudo-random	0–100	Undocumented	Undocumented
	VT270-200	–4.31	Pseudo-random	0–100	Undocumented	Undocumented
8	VT315	–4.31	Pseudo-random	0–100	Undocumented	Undocumented
	VT315-200	–4.31	Pseudo-random	0–100	Undocumented	Undocumented
9	IP270-A10[4]	–139.7	Pseudo-random	0–100	400	Hanning Broad
10	IP270NVP[5]	–139.7	Pseudo-random	0–100	400	Hanning Broad
11	IP000NVP	–49.2	Pseudo-random	0–100	Undocumented	Undocumented

1. IP is in-plane; VT is vertical shaking. Number indicates azimuth of shaker location. Input load is positive in tension (i.e., towards the reaction mass).
2. –200 indicates additional 200 lb of weight present on the shake plate.
3. VTC is vertical shaking on center.
4. –A10 indicates shaking at an alpha of –10 deg.
5. NVP indicates vertical shake plate not present.

Table A4. Vertical shake plate rap test hammer and accelerometer directions.

Point	Rap Azimuth (deg)	Accel Direction (deg)
1	180	0
2	270	270
3	225	0
4	225	270
5	Vertical*	Up

* Vertical hammer strike on top of the vertical shake plate near the center.

Shaft Bending Gauge Equations

Bending gauge moments:

MRSEBL	Shaft extender bending, primary (in-lb)
MRSEBLB	Shaft extender bending, backup (in-lb)
MRSBM	Lower shaft bending, primary (in-lb)
MRSBMB	Lower shaft bending, primary (in-lb)

Rotating forces and moments:

$$ROTF1 = \frac{0.96MRSBM - MRSEBLBsin(9°) - MRSEBLcos(9°)}{13.716}$$

$$ROTF2 = \frac{MRSEBLBcos(9°) - MRSEBLsin(9°) - 0.96MRSBMB}{13.716}$$

$$ROTM1 = \frac{1.889\big(MRSEBLBcos(9°) - MRSEBLsin(9°)\big) - 0.726MRSBMB}{13.716}$$

$$ROTM2 = \frac{1.889(MRSEBLBsin(9°) + MRSEBLcos(9°) - 0.726MRSBM}{13.716}$$

Fixed-system forces and moments in hub axes:

$$Axial\ Force\ (lb) = ROTF1\cos(AZ - 5.2°) - ROTF2\sin\ (AZ - 5.2°)$$

$$Side\ Force\ (lb) = ROTF1\sin(AZ - 5.2°) + ROTF2\cos\ (AZ - 5.2°)$$

$$Pitching\ Moment\ (ft - lb) = ROTM1\sin(AZ - 5.2°) + ROTM2\cos\ (AZ - 5.2°)$$

$$Rolling\ Moment\ (ft - lb) = -ROTM1\cos(AZ - 5.2°) + ROTM2\sin\ (AZ - 5.2°)$$

AZ is the hub azimuth, given in Table A3.

APPENDIX B. ACCELEROMETER AND NASTRAN MODE SHAPES

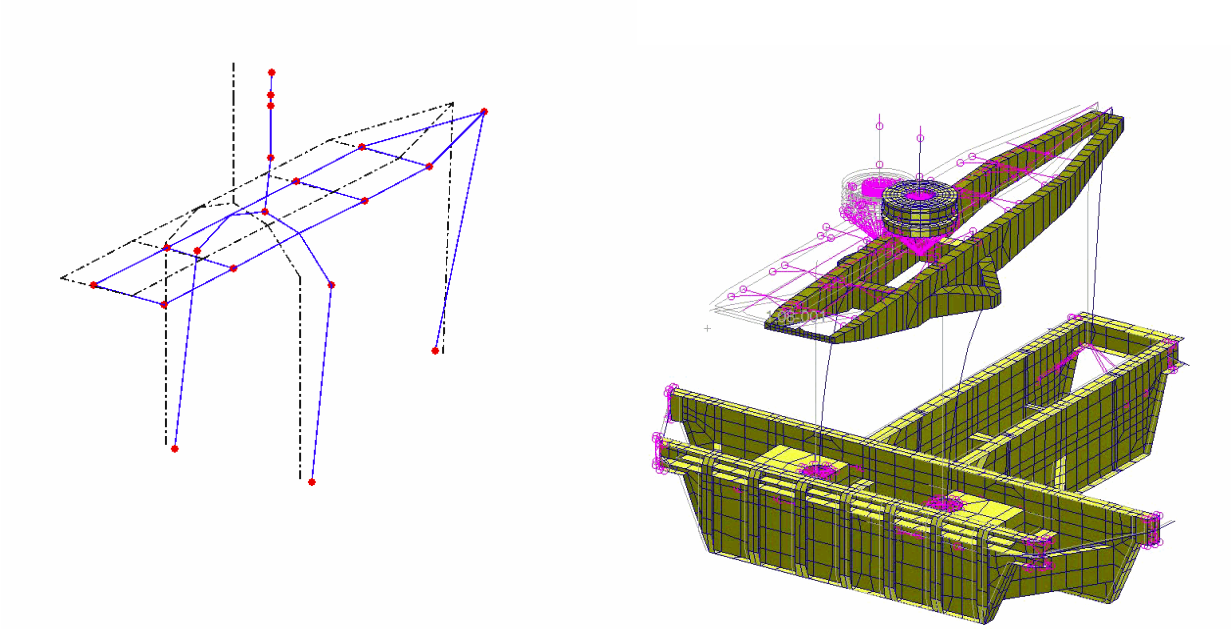

(a) Accelerometer data (scale 2×10^{6})—1.7 Hz **(b) NASTRAN prediction—2.4 Hz**

Figure B1. Comparison of accelerometer data and NASTRAN model—Mode 1.

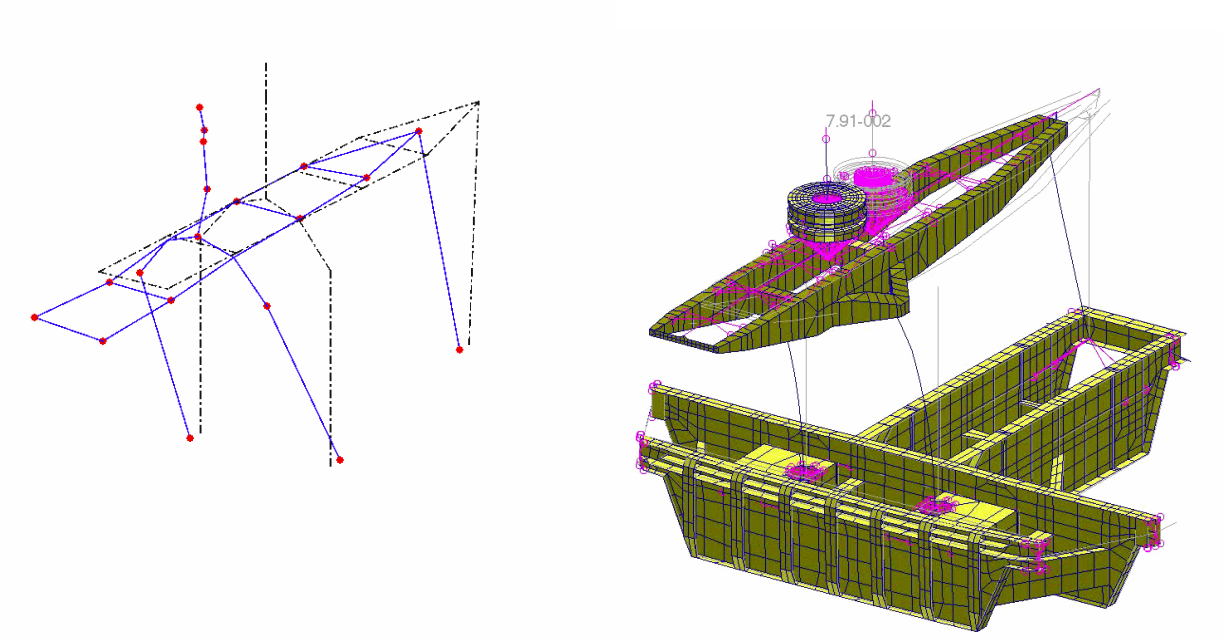

(a) Accelerometer data (scale 10^{6})— 2.3 Hz **(b) NASTRAN prediction—2.4 Hz**

Figure B2. Comparison of accelerometer data and NASTRAN model—Mode 2.

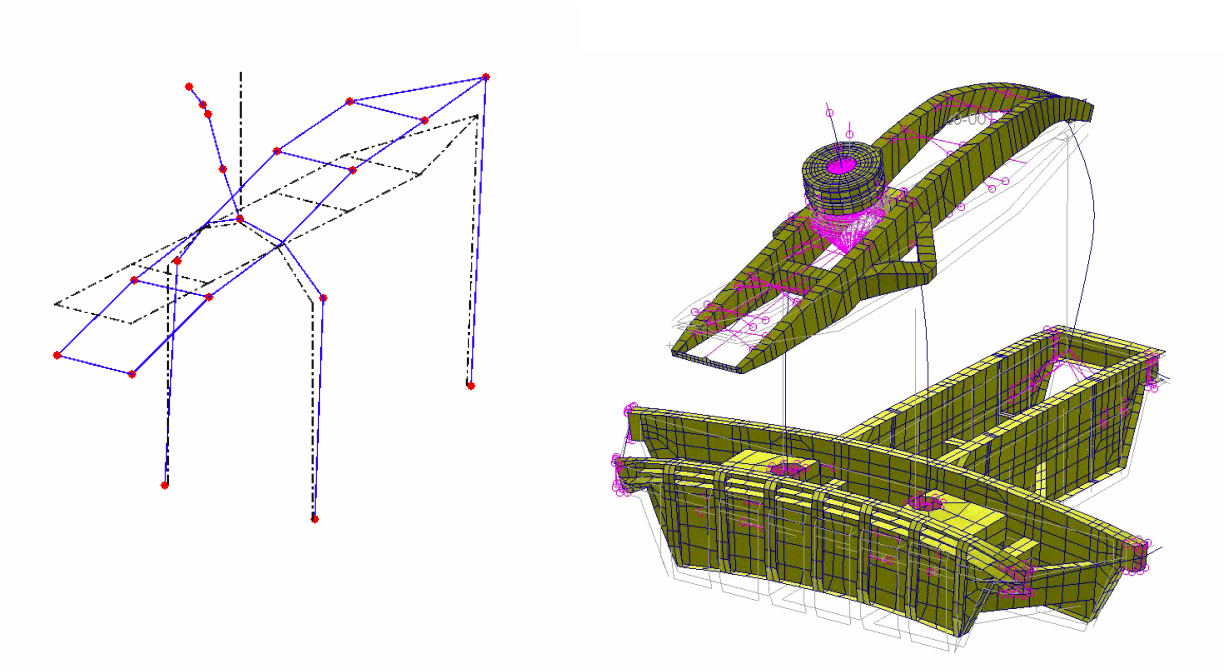

(a) Accelerometer data (scale 10^7)—9.3 Hz **(b) NASTRAN prediction—13.4 Hz**

Figure B3. Comparison of accelerometer data and NASTRAN model—Mode 4.

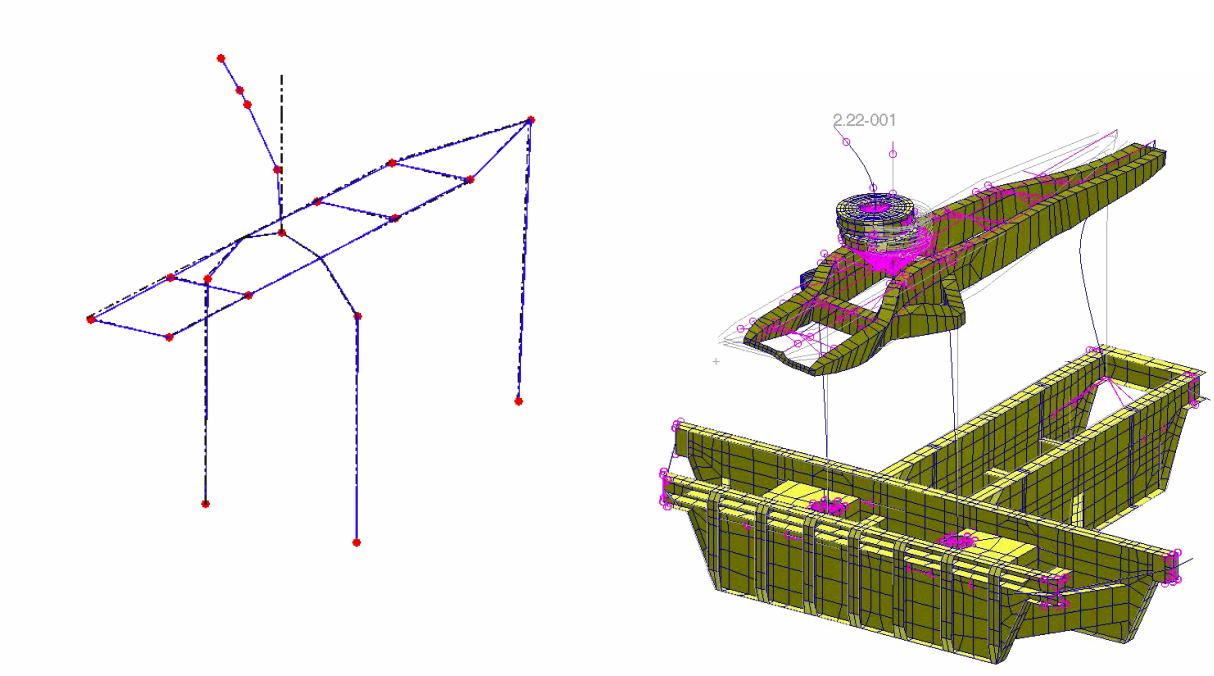

(a) Accelerometer data (scale 10^6)—15.9 Hz **(b) NASTRAN prediction—26.1 Hz**

Figure B4. Comparison of accelerometer data and NASTRAN model—Mode 5.